

SuperServe: Fine-Grained Inference Serving for Unpredictable Workloads

Alind Khare¹, Dhruv Garg¹, Sukrit Kalra², Snigdha Grandhi*³, Ion Stoica², and Alexey Tumanov¹

¹Georgia Tech ²UC Berkeley ³Adobe
 {alindkhare, dgarg39, sgrandhi32, atumanov}@gatech.edu
 {sukrit.kalra, istoica}@berkeley.edu

Abstract

The increasing deployment of ML models on the critical path of production applications in both datacenter and the edge requires ML inference serving systems to serve these models under unpredictable and bursty request arrival rates. Serving models under such conditions requires these systems to strike a careful balance between the latency and accuracy requirements of the application and the overall efficiency of utilization of scarce resources. State-of-the-art systems resolve this tension by either choosing a static point in the latency-accuracy tradeoff space to serve all requests or load specific models on the critical path of request serving.

In this work, we instead resolve this tension by simultaneously serving the entire-range of models spanning the latency-accuracy tradeoff space. Our novel mechanism, SubNetAct, achieves this by carefully inserting specialized operators in weight-shared SuperNetworks. These operators enable SubNetAct to dynamically route requests through the network to meet a latency and accuracy target. SubNetAct requires upto $2.6\times$ lower memory to serve a vastly-higher number of models than prior state-of-the-art. In addition, SubNetAct’s near-instantaneous actuation of models unlocks the design space of fine-grained, reactive scheduling policies. We explore the design of one such extremely effective policy, SlackFit and instantiate both SubNetAct and SlackFit in a real system, SuperServe. SuperServe achieves 4.67% higher accuracy for the same SLO attainment and $2.85\times$ higher SLO attainment for the same accuracy on a trace derived from the real-world Microsoft Azure Functions workload and yields the best trade-offs on a wide range of extremely-bursty synthetic traces *automatically*.

1 Introduction

Recent advancements in machine-learning (ML) techniques have unlocked vast improvements in both accuracy and efficiency of a variety of tasks such as image classification [38],

object detection [3, 8], text summarization [16], sentiment analysis [29], next word prediction [47] etc. As a result, ML models have been quickly deployed across a wide-range of applications in both datacenters [23, 37, 41, 46, 61] and on the edge [4, 17, 33, 39], and are now subject to the stringent requirements of a production application.

Notably, ML models on the critical-path of these applications must now deal with *unpredictable* request rates that rapidly change at a sub-second granularity. For example, web applications in datacenters increasingly rely on ML models [46, 61], and are known to have extremely bursty request rates, with a peak demand that is $50\times$ higher than the average [32]. Similarly, request rates in autonomous vehicles change rapidly as a function of various factors such as the terrain (city vs. freeway driving), time of the day etc. [17].

Thus, ML inference serving systems have the arduous task of striking a careful balance between three key requirements of production applications facing unpredictable request rates: **R1: Latency.** ML models are being increasingly deployed in applications that have extremely stringent latency requirements, quantified using a Service-Level Objective (SLO) [31]. For example, both web serving [22, 41, 46] in datacenters and autonomous vehicles [17, 33] on the edge must maximize the number of requests completed within the specified SLO ranging from 10s to 100s of milliseconds [17, 59].

R2: Accuracy. Techniques such as Neural Architecture Search (NAS) [5, 48, 62] have enabled the development of multiple ML models that offer varying accuracies for a particular task. As a result, applications demand the highest-accuracy results possible within the latency targets of their requests. For example, increased accuracy has been intricately tied to a better user experience for web applications [23, 54]. Similarly, the safety of an autonomous vehicle heavily relies on the accuracy of various different ML models [17, 18].

R3: Resource-Efficiency. Web applications at Facebook process 200 trillion ML model requests daily [51], which represents a significant fraction of Facebook’s datacenter demands [41]. In addition to the increasing proliferation of ML models, their growing reliance on scarce resources such as

*Work done as a student at Georgia Tech

GPUs and specialized accelerators (e.g, TPUs [1], AWS Inferentia [2]) for efficient inference has led to resource tensions across applications in both datacenters and on the edge [39]. Thus, inference serving systems that serve a wide range of ML models must make judicious use of these scarce resources.

The first-generation of inference serving systems [10,11,22,30,36,37,59] resolves this tension by choosing a static point in the tradeoff-space between **R1-R3** and serving all requests using the same model for the entirety of the application’s runtime. As a result, applications must make a one-time decision to forego meeting their SLO targets (**R1**) under bursty request rates or suffer degraded accuracy (**R2**) under normal conditions. More recently, state-of-the-art inference serving systems [42,60] enable applications to register multiple ML models spanning the entire pareto frontier of latency (**R1**) and accuracy (**R2**) targets, and *automatically* choose the appropriate model to serve requests based on the incoming request rates. These systems must either keep the entire set of models in memory or rely on *model switching* techniques to load the required models at runtime [60]. As GPU memory remains the key resource bottleneck in both datacenter and edge inference serving [32,39], these systems must now choose between **R3** – effectively utilizing the available resources (by incurring the enormous latency penalties of switching models), or **R1** – meeting SLO targets under highly unpredictable request rates.

Conventional wisdom in inference serving literature touts the “*non-negligible provisioning time* [for ML models due to switching], *which can exceed the request processing times*” as a “*key characteristic of ML workloads*”, and “*rules out reactive techniques*” for responding to bursty request rates [21]. This wisdom has been widely accepted [11,22,42] leading to the development of coarse-grained scheduling policies for inference serving that must account for the enormous latency penalty of switching models when reacting to bursty request rates. As a result, these coarse-grained policies typically avoid or minimize switching models by design [42], and are hence, unable to optimally navigate the tradeoff space between **R1-R3** under rapidly-changing, unpredictable request rates.

In this work, we challenge this conventional wisdom that forces a choice between **R1** and **R3**. We describe a mechanism, SubNetAct, to simultaneously serve the entire range of models spanning the latency-accuracy tradeoff space (**R1-R2**) in a resource-efficient manner (**R3**). At the core of our mechanism are novel control-flow and slicing operators that SubNetAct carefully inserts into the SuperNet [6,44] neural architectures. SuperNets enable a latency-accuracy tradeoff (**R1-R2**) by training a set of shared model weights for many neural networks, without duplication. Prior works [6,44] propose efficient mechanisms for training SuperNets for both vision and NLP tasks, but require each model instance to be individually extracted for inference, leading to a similar choice as before between **R1** and **R3** – either load all individual models or switch between them at runtime. However, SubNetAct’s novel operators obviate the need to extract individual models

and load them dynamically at runtime. Instead, SubNetAct dynamically routes requests within one SuperNet deployment with negligible overhead, enabling near-instantaneous *actuation* of different models. As a result, SubNetAct unlocks orders of magnitude improvements in the navigation of the latency-accuracy tradeoff-space (**R1-R2**), while substantially reducing the memory footprint (**R3**) (see §2.2).

In addition to being resource-efficient (**R3**), SubNetAct’s agility in navigating the latency-accuracy tradeoff space (**R1-R2**) fundamentally changes the design space of scheduling policies. Instead of complex scheduling policies that must reason about future request rates in a bid to avoid paying the latency of switching ML models dynamically under bursts, SubNetAct enables the specification of simple policies that directly optimize for the key success metrics **R1-R3**. While conventional wisdom deems such reactive policies infeasible, we explore one example point in this design space with a simple, yet effective policy that we call SlackFit. SlackFit is a reactive scheduling policy that exploits the near-instantaneous actuation property of SubNetAct to make fine-grained decisions about how many requests to serve in a batch, and which latency/accuracy choice to select for serving in real-time.

We summarize the contributions of this paper as follows:

- We introduce SubNetAct (§3.1), a novel mechanism that enables a resource-efficient, fine-grained navigation of the latency-accuracy tradeoff space. SubNetAct achieves this by carefully inserting novel control-flow and slicing operators that dynamically route requests through a single SuperNet.
- We unlock the design space of fine-grained, reactive scheduling policies and provide a mathematical formulation of their objective (§4.1). We then propose SlackFit (§4.2), a simple, yet effective greedy heuristic and show how it accurately approximates the optimal objective.
- We instantiate SubNetAct and SlackFit in a real-world system, SuperServe, a real-time asynchronous model serving system with pluggable scheduling policies (§5).
- We extensively evaluate SuperServe with both SlackFit and several state-of-the-art scheduling policies (§6). We find that SuperServe achieves 4.67% higher accuracy for the same SLO attainment and 2.85× higher SLO attainment for the same accuracy on the real-world Microsoft Azure Functions trace.

2 Motivation and Background

In §2.1, we motivate the development of a reactive, fine-grained scheduling policy that maximizes **R1-R3** under unpredictable, bursty request rates. §2.2 then provides a background on SuperNets [6,44] and discusses the properties of SuperNets relevant to **R1-R2** that make them a good fit for a fine-grained exploration of the latency-accuracy tradeoff.

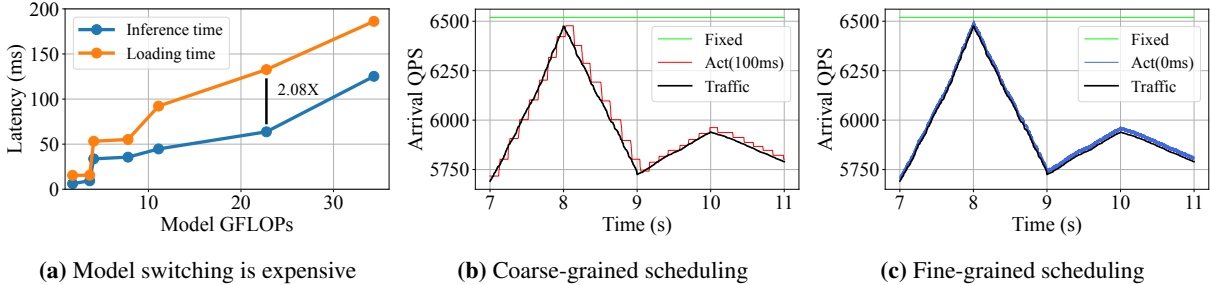


Fig. 1: Fine-grained scheduling policies are beneficial. (a) The latency of loading ResNet-18,34,50,101,152 [24], Wide-Resnet-101 [58] and ConvNeXt-Large [35] is greater than its inference latency with a batch size of 16, making model switching expensive. This gap widens as model sizes increase. (b) A bursty request rate from the MAF [45] trace with a coarse-grained scheduling policy leads to 2% of the requests missing their SLO (**R1**) and wasting resources (**R3**) due to a 100ms actuation delay typical of model switching techniques. (c) A bursty request rate with a fine grained scheduling policy that can switch models instantaneously can achieve 0% SLO misses and effectively utilizes the GPU.

2.1 Fine-Grained Reactive Scheduling

Prior works in inference serving systems [32, 59] have exhaustively analyzed both production traces from Microsoft Azure Functions (MAF) [45] and synthetic application traces with a goal of highlighting their bursty request arrival patterns. For example, Zhang et al. [59] underscore the high coefficient of variance in request arrivals in production traces [45]. Further, the authors claim that the bursty “*sub-second request arrival patterns [are] nearly impossible to predict*”, thus frustrating the goal of meeting the stringent SLO requirements of requests in an ML-based production applications.

A strawman solution to fulfilling SLOs under bursty request rates requires inference serving systems to provision for the peak. In this setting, these systems load the entire set of models spanning the latency-accuracy tradeoff space into GPU memory and switch between them as request rate fluctuates. While this reduces the actuation latency of switching models, allowing inference serving systems to rapidly degrade accuracy (**R2**) under bursts to meet SLO targets (**R1**), it wastes resources under normal request rates (**R3**).

As a result, state-of-the-art inference serving systems [42, 60] rely on model switching techniques that page models in and out when required, to make efficient use of GPU memory (**R3**). However, as we show in Fig. 1a, the loading time of ML models from CPU to GPU memory is vastly more than the inference time of the biggest batch size, and the gap widens as the model sizes increase. Thus, in a bid to offset the cost of loading models on the critical path of handling requests, inference serving systems rely on *predictive* scheduling policies that make coarse-grained estimations of future request arrival patterns. Such policies are bound to be suboptimal owing to the difficulty of predicting the short bursts in request arrival rates coupled with their stringent SLO requirements [59].

We believe that the key to optimally serving bursty request rates instead lies in the ability to rapidly switch between ML models thus obviating the need for coarse-grained predictive scheduling policies. To validate our hypothesis, we simulate a coarse-grained policy with an actuation delay (i.e., time taken

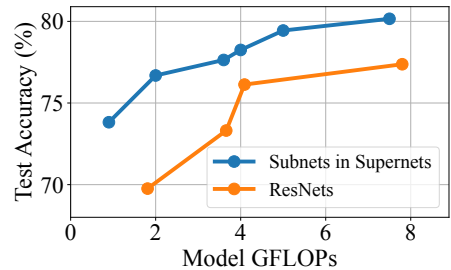


Fig. 2: Supernet provide better latency-accuracy tradeoff. The accuracy (**R2**) of subnets individually extracted from OFAResNet supernet [6] is vastly superior to the hand-tuned ResNets from Fig. 1a for the same FLOP requirements (**R1**).

to switch to a new ML model that can handle the current request rate) of 100ms and an idealistic fine-grained policy with an actuation delay of 0ms. Figs. 1b and 1c plot the effects of these policies on a small bursty subtrace from the MAF trace. We observe that the coarse-grained policy leads to higher SLO misses (**R1**) under increasing request rates and wasted resources (**R3**) under decreasing request rates. On the other hand, the fine-grained policy is able to instantaneously adjust to the increasing and decreasing request rates leading to no missed SLOs and effective utilization of the GPU.

2.2 Weight-Shared Supernets

The problem of navigating the pareto-optimal frontier of the latency-accuracy tradeoff space (**R1-R2**) by finding highest accuracy DNNs for a specific latency target is well studied in ML literature. Conventional Neural Architecture Search (NAS) [7, 34, 48, 62, 63] approaches have enabled architectures tailored to a particular latency target. However, these approaches search for and train individual networks for a particular latency target and hence require inference serving systems to either load all of them into memory and waste resources (**R3**), or switch between them at runtime.

Instead, recent works [6, 44] have proposed first training one *supernet* and then extracting a subset of its layers to form

subnets. As a result, once the supernet is trained, no further retraining is required for a specific subnet. Each extracted subnet targets a specific point in the latency-accuracy tradeoff space, and partially shares its weights/layers with other subnets. In addition, this automated neural architecture search (NAS) yields subnets that correspond to vastly superior points in the latency-accuracy tradeoff space (**R1-R2**). For example, Fig. 2 highlights the accuracy benefits of subnets extracted from a ResNet-based supernet when compared to the hand-tuned ResNets for an equivalent number of FLOPs.

In order to find subnets that target a particular point in the latency-accuracy tradeoff space, the architecture search in supernet relies on the following parameters: - (i) *Depth* (\mathbb{D}) describes the depth of a subnet, (ii) *Expand Ratio* (\mathbb{E}) describes layer-wise ratio of output to input channels of a convolution or fully-connected layer, and (iii) *Width Multiplier* (\mathbb{W}) describes layer-wise fraction of input and output channels to be used. These parameters (\mathbb{D} , \mathbb{E} , \mathbb{W}) combinatorially create an architecture space, Φ ($|\Phi| \approx 10^{19}$) [6], from which individual subnets are extracted *statically* for inference.

3 SubNetAct: Instantaneous Model Actuation

Motivated by §2.1, we seek to develop a fine-grained, reactive scheduling mechanism that enables efficient execution of ML-based production applications (**R1-R3**) under bursty request rates. As discussed in §2.2, prior work in supernet [6, 44] enables the extraction of individual models that target a specific point in the latency-accuracy tradeoff space (**R1-R2**). However, these approaches yield individual models that must either be simultaneously deployed (wasting resources; **R3**) or paged in as request rates fluctuate (missing SLOs; **R1**).

To resolve this fundamental tension, we make the key observation that by virtue of performing architectural search *post* training, a supernet subsumes the entire architectural space of subnets. As a result, instead of extracting and deploying individual subnets (as done previously), we can instead deploy a supernet and *dynamically route* requests to the appropriate subnet. This observation leads us to introduce SubNetAct, a memory-efficient model *actuation* mechanism (**R3**) that exposes fine-grained control decisions to near-instantaneously switch between subnets in order to pick the optimal point in the latency-accuracy tradeoff space (**R1-R2**).

SubNetAct’s (Fig. 3) key insight lies in the introduction of the following three novel operators that enable it to dynamically route requests to the required subnet in a supernet:

LayerSelect. SubNetAct takes as input the depth \mathbb{D} , and dynamically executes layers of a specific subnet based on \mathbb{D} . The depth \mathbb{D} is converted by SubNetAct to per-layer boolean values that determine which layers participate in inference. SubNetAct then wraps each layer in a LayerSelect operator that enforces control-flow by either passing the input activation to the wrapped layer or skipping the layer and directly forwarding input to the next layer. This operator enables layer-

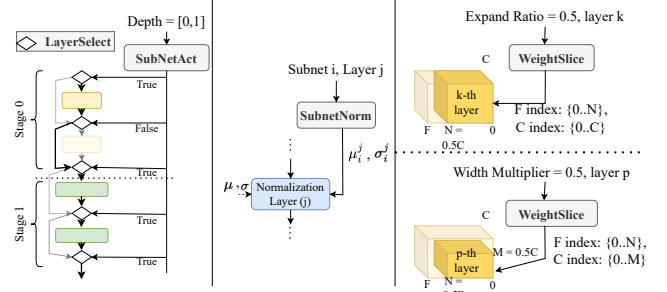


Fig. 3: SubNetAct’s novel operators (LayerSelect, SubNetNorm, WeightSlice) dynamically actuate subnets by routing requests through weight-shared layers and non-weight-shared components.

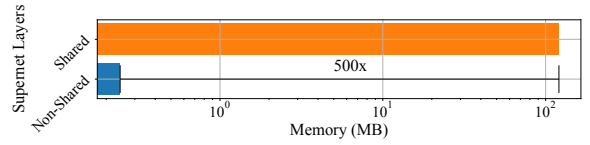


Fig. 4: SubNetAct’s memory savings. The memory used by the normalization statistics is $500\times$ smaller than the non-normalization layers. SubNetNorm decouples the normalization statistics for each subnet and provides accurate bookkeeping thus enabling high accuracy (**R1**), with minimal increase in memory consumption (**R3**).

sharing among subnets that differ in depth ($\Phi_{\mathbb{D}} \subset \Phi$), which reduces the GPU memory consumption of the supernet (**R3**). Moreover, it enables near-instantaneous (**R1**) switching of the supernet’s accuracy (**R2**) under bursty request rates.

SubnetNorm. We observe that naively introducing the LayerSelect operator leads to a significant drop in subnet accuracy (as low as 10%). This is due to the incorrect tracking of the mean (μ) and variance (σ) in normalization layers such as BatchNorm [27]. To account for this discrepancy, SubNetAct introduces the SubnetNorm operator that precomputes and stores μ and σ for each possible subnet by performing forward pass inference on the training data. SubnetNorm takes as input a unique subnet ID (i) and a layer ID (j) and outputs the precomputed normalization statistics $\mu_{i,j}$ and $\sigma_{i,j}$. The layer j then uses the provided statistics to perform normalization of activations, effectively specializing j for each subnet i .

Although this bookkeeping increases the memory requirements of deploying the supernet, Fig. 4 shows that the overhead of these non-shared normalization statistics is $500\times$ smaller than the memory requirement of the shared layers. As a result, SubNetAct can host thousands of subnets in memory by only keeping the statistics unique to each subnet and sharing the non-normalization weights amongst all the subnets.

WeightSlice. This operator dynamically selects channels in convolution or fully-connected layers during inference. The input to WeightSlice is the expand ratio (\mathbb{E}) or width multiplier (\mathbb{W}) for each layer, which collectively determine the number of channels to be used. The operator outputs layer-specific channel indices, which are then used to select weight subsets for the forward pass inference. The operator enables

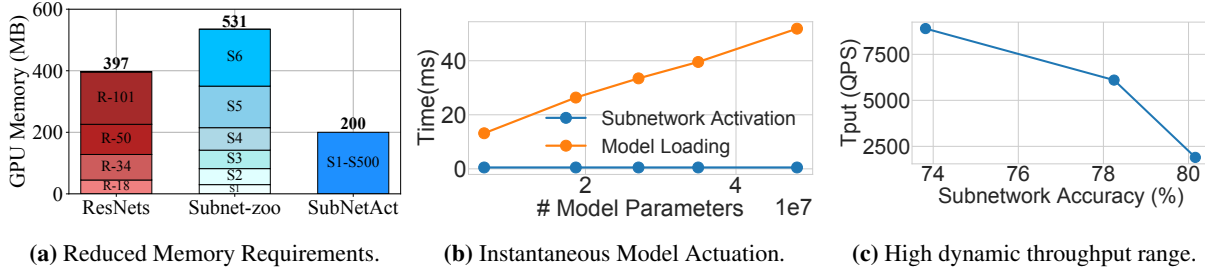


Fig. 5: Efficacy of SubNetAct. (a) SubNetAct requires upto $2.6\times$ lower memory to serve a higher-range of models when compared to the ResNets from Fig. 1a and six individual subnets extracted from supernet [6] (b) SubNetAct actuates different subnets near-instantaneously ($< 1\text{ms}$), which is orders of magnitude faster than the model switching time. (c) SubNetAct enables instantaneous actuation of models that can sustain higher ingest rates thus inducing a wide dynamic throughput range ($\approx 2 - 8k$ queries per second) and increased accuracy.

partial layer-sharing among subnets ($\{\Phi_{\mathbb{E}} \cup \Phi_{\mathbb{W}}\} \subset \Phi$), thus increasing the number of available subnet architectures. As a result, SubNetAct is able to provide the entire set of latency-accuracy options (**R1-R2**) to the scheduling policies.

We note that the input to these operators (i.e., depth (\mathbb{D}), expand ratio (\mathbb{E}) and width multiplier (\mathbb{W})) remains similar to the inputs for architectural search in ML literature [6]. Moreover, these control inputs are independent from the input to the actuated subnet (i.e., the request served by the model), and are declaratively specified by a scheduling policy (§5). Given the arrival rate, the scheduling policy chooses a specific subnet for a request (by specifying the control tuple \mathbb{D} , \mathbb{E} and \mathbb{W}), which is then actuated by SubNetAct near-instantaneously.

3.1 Discussion: Efficacy of SubNetAct

We now highlight SubNetAct’s efficacy in achieving key application requirements (**R1-R3**) under bursty request rates.

Reduced Memory Requirements. SubNetAct’s novel operators enable subnets to share layers in place and dynamically route requests to the appropriate subnet based on the control tuple \mathbb{D} , \mathbb{E} and \mathbb{W} determined by a scheduling policy. As a result, SubNetAct can simultaneously serve the entire range of models spanning the latency-accuracy tradeoff space while drastically reducing memory requirements. Fig. 5a demonstrates this by comparing the memory requirement of loading four different ResNets [24], six individually extracted subnets [6], and SubNetAct that enables simultaneous actuation of 500 subnets. We observe that SubNetAct can reduce memory consumption by upto $2.6\times$, while vastly increasing the latency-accuracy tradeoff points that can be actuated.

Near-Instantaneous Model Actuation. While switching between individual models requires loading their weights to the GPU, SubNetAct’s operators enable scheduling policies to actuate any subnet *in place* without incurring additional loading overhead. Fig. 5b compares the time taken to perform on-demand loading of individual subnetworks versus in-place actuation of a subnet in SubNetAct. We observe that SubNetAct’s model actuation is orders-of-magnitude faster than on-demand loading of ML models. This allows scheduling

policies that use SubNetAct to rapidly actuate lower-accuracy models under bursty conditions (**R1**) and switch to higher-accuracy models under normal load (**R2**), without coarse-grained predictions about future request rates.

Increased Throughput & Accuracy. By providing instant model actuation, SubNetAct allows scheduling policies to scale the throughput of the system up and down rapidly, thus inducing a broad throughput range within as few as 6% of accuracy to help meet SLO guarantees (**R1-R2**). Fig. 5c compares the maximum sustained ingest throughput for a point-based open-loop arrival curve for serving the largest, smallest, and a median subnetwork on 8 SubNetAct workers. We observe that SubNetAct can serve a wide throughput range from 2000-8000 QPS, while being able to instantaneously increase accuracy between 74% to 80%.

4 Fine-Grained Scheduling Policies

SubNetAct’s near-instantaneous actuation of the entire latency-accuracy tradeoff space unlocks the development of extremely fine-grained scheduling policies that can directly optimize for **R1-R2**. We note that by virtue of aggressively sharing weights/layers and dynamically routing requests within a supernet, SubNetAct automatically maximizes resource efficiency (**R3**). In this section, we first start with the problem formulation of online serving for the new space of fine-grained policies enabled by SubNetAct (§4.1). We then describe our proposed policy SlackFit that aims to achieve both high accuracy and latency SLO attainment (§4.2).

4.1 Problem Formulation

SubNetAct hosts a set of all possible subnets Φ , where each subnet $\phi \in \Phi$ is defined by the control tuple \mathbb{D} , \mathbb{E} , \mathbb{W} and has an accuracy $Acc(\phi)$ and a latency-profile $l_{\phi}(B)$ as a function of batch-size B . A query¹ q arrives to the scheduler at time a_q with an SLO d_q . A fine-grained scheduling policy focuses on selecting a subnet across supernets for queries across GPUs, along with a batch B to execute the query in [11, 22]. The

¹We use the term *query* and *request* interchangeably.

arrival time $a(B)$ of B is the earliest arrival time and the deadline $d(B)$ is the earliest deadline of all queries in B . \mathcal{B} is the set of all possible batches of queries. The policy decides if $B \in \mathcal{B}$ should execute at time t using subnet ϕ on GPU n , which is captured by a decision variable $I(B, t, n, \phi) \in \{0, 1\}$. **Goal.** The policy’s goal is to maximize the number of accurate responses (to queries) within specified SLO (**R1-R2**).

Optimal Offline ILP. We now present the ILP formulation of a scheduling policy that achieves our stated goal with an oracular knowledge about future query arrivals:

$$\text{maximize } \sum_t \sum_n \sum_{\phi \in \Phi} \sum_{B \in \mathbb{B}} \text{Acc}(\phi) \cdot |B| \cdot I(B, t, n, \phi) \quad (1)$$

$$\text{s.t. } \sum_t \sum_n \sum_{\phi \in \Phi} \sum_{\{B|q \in \mathbb{B}\}} I(B, t, n, \phi) \leq 1, \quad \forall q \quad (1a)$$

$$\sum_{B \in \mathbb{B}} \sum_{\{t' \leq t \leq t' + l_\phi(B)\}} I(B, t', n, \phi) \leq 1, \quad \forall n, t, \phi \quad (1b)$$

$$a(B) \cdot I(B, t, n, \phi) \leq t, \quad \forall n, t, B, \phi \quad (1c)$$

$$\sum_{\phi \in \Phi} I(B, t, n, \phi) \leq 1, \quad \forall n, t, B \quad (1d)$$

$$\sum_{\phi \in \Phi} (l_\phi(B) + t) \cdot I(B, t, n, \phi) \leq d(B), \quad \forall n, t, B \quad (1e)$$

$$I(B, t, n, \phi) \in \{0, 1\}, \quad \forall n, t, B, \phi \quad (1f)$$

The ILP maximizes the number of queries that satisfy their latency SLOs with the highest possible accuracy across all the selected query batches i.e., $\exists \phi : I(B, t, n, \phi) = 1$ and $\text{Acc}(\phi) \cdot |B|$ is maximized. The constraints of the ILP denote -

- (1a) A query q can be assigned to at-most one batch B .
- (1b) A GPU n can only execute a single subnet ϕ on a single batch B at a particular time t .
- (1c) Batch B can only execute after its arrival time $a(B)$.
- (1d) Each batch B can be served with a maximum of one subnet ϕ on a GPU n at a time t .
- (1e) The batch should complete before deadline $d(B)$.
- (1f) The choice variable $I(B, t, n, \phi)$ is a boolean indicator.

We note that our formulation (1) is a Zero-one Integer Linear Program (ZILP) and solving it is known to be NP-Hard [40, 59]. Furthermore, it is impractical to expect oracular query arrival knowledge. This renders the use of the formulated ILP in the online model serving setting unrealistic. Instead, we approximate its behavior under different query traffic conditions with an *online* scheduling policy instead.

4.2 SlackFit: Online-Scheduling Policy

We introduce SlackFit—a simple yet effective online scheduling policy that aims to maximize accuracy and latency SLO (**R1-R2**). SlackFit is a greedy heuristic that approximates the ILP-based policy in Eq. (1) and makes the decision-making tractable. SlackFit makes following design choices:

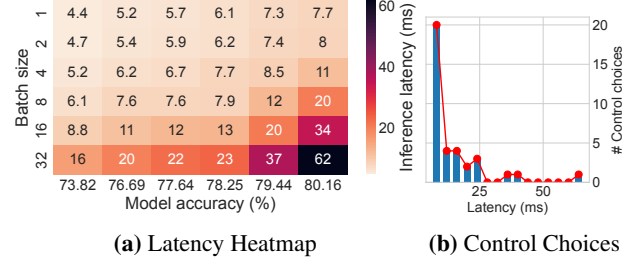


Fig. 6: SlackFit control parameter space. (a) latency heatmap for six different (uniformly sampled w.r.t. FLOPs) pareto-optimal subnets in SubNetAct as a function of accuracy (x-axis) and batch size (y-axis). The latency is *monotonic* with batch size and accuracy. (b) the number of available choices decrease as latency increases.

Operates on Pareto-Optimal Subnets (Φ_{pareto}). To make subnet choices in reasonable time, SlackFit operates on the Φ_{pareto} instead of Φ . Φ_{pareto} is a set of pareto-optimal subnets w.r.t. latency, accuracy obtained by using existing neural architecture search (NAS) methods [6]². The size of $|\Phi_{\text{pareto}}| \approx 10^3$ is orders of magnitude smaller than $|\Phi| \approx 10^{19}$. This contributes to rapid scheduling decisions in SlackFit.

Uses Monotonic Properties of Subnets in Φ_{pareto} . SlackFit leverages key properties of subnets in Φ_{pareto} to further reduce the control search space by performing $O(\log)$ operations. Fig. 13a shows latency profiles of six subnets uniformly sampled w.r.t. FLOPs from Φ_{pareto} . The properties of subnets in Φ_{pareto} are - **(P1)** the latency increases monotonically with batch size, **(P2)** the latency increases monotonically with accuracy, **(P3)** the latency difference among different batch sizes of a subnet increases with increase in subnet accuracy.

Properties **P1** and **P2** further reduce the dimensionality of control search for SlackFit to a single dimension (i.e., latency) to determine both the subnet ϕ and batch size B . Instead of searching the two-dimensional table (Fig. 13a), SlackFit operates on one-dimensional set of evenly sized latency buckets (Fig. 13b). Each bucket consists of control tuples (B, ϕ) such that $l_\phi(B)$ remains within the range of bucket width. Buckets are constructed to exploit **P3** and to further reduce the search complexity to $O(1)$ for bucket selection. By construction and property **P3**, low latency buckets contain lower accuracy, higher throughput control choices, as the inference latency of smaller accuracy subnets on higher batch sizes is relatively lower. High latency buckets contain higher accuracy, lower throughput control choices.

Slack-Based Decision-making. SlackFit’s insight is that the remaining slack of the most urgent query provides proxy to changes in the traffic. Traffic peaks lead to more queuing delays in the system and in-turn reduces the remaining slack. Under low traffic, the slack remains high. Therefore, SlackFit uses remaining slack for decision making. It chooses a bucket with latency that is closest to and less than the remaining slack of the most urgent query. All control choices within

²It takes ≤ 2 min to perform NAS on supernet by using latency and accuracy predictors

the bucket satisfy query deadline. It picks the control choice with maximum batch size to opt for a high throughput choice especially for lower slack (traffic peaks).

SlackFit Behavior. With slack-based decision making, SlackFit can automatically adjust accuracy (**R2**) and throughput of the system by choosing appropriate latency bucket on variable arrival traffic to maintain high SLO (**R1**). A well-behaved trace (e.g., low ingest rate, variation) results in higher slack. Higher slack leads to the choice of higher latency buckets. And, higher latency buckets are correlated strongly with the probability of choosing higher accuracy models (due to property **P2**). Conversely, bursty traces lead to lower latency bucket choices, as SlackFit operates under reduced latency slack. Lower latency bucket choices have higher batch sizes configuration (due to property **P3**). Thus, SlackFit opportunistically maximizes accuracy while satisfying latency SLO.

4.2.1 SlackFit Approximation of Optimal Offline ILP

We now provide insights on how SlackFit emulates behavior of the optimal offline ILP. To understand the behavior of ILP, we formulate a proxy utility function that captures the inner-term of the ILP objective function in Eq 1, the utility function is defined for all subnet ϕ , batch-size B and a deadline d_B (earliest deadline of queries in batch) –

$$\mathbb{U}(\phi, B, d_B) = \begin{cases} \text{Acc}(\phi) \cdot |B|, & \text{if } l_\phi(B) < d_B \\ 0, & \text{otherwise} \end{cases} \quad (2)$$

The utility in Eq. 2 is non-zero if and only if subnet ϕ performs batch-inference on batch B within the deadline d_B , and is zero otherwise. Note that this captures the success metrics: maximizing both the number of queries processed (**R1**) within their deadline and the accuracy they were served with (**R2**).

A. Offline ILP and SlackFit Prefer Pareto-Optimal Subnets. SlackFit’s key design choice is to operate pareto-optimal subnets w.r.t. latency, accuracy (Φ_{pareto}) (§4.2). We claim that offline ILP also tends to pareto-optimal subnets (w.r.t. latency, accuracy), as these subnets yield higher utility.

Lemma 4.1. *The utility of pareto-optimal subnets is higher than non-pareto-optimal subnets if they have similar inference latency for a batch of queries.*

$$\mathbb{U}(\phi_p, B, d_B) > \mathbb{U}(\phi_q, B, d_B), \quad \forall B, d_B \\ \text{s.t. } \phi_p \in \Phi_{\text{pareto}}, \phi_q \in \{\Phi \setminus \Phi_{\text{pareto}}\}, l_{\phi_p}(B) \approx l_{\phi_q}(B)$$

This validates SlackFit’s design choice to operate on pareto-optimal subnets only. We defer the proof to Appendix §A.1.

B. Offline ILP and SlackFit Prioritize Lower Accuracy & Higher Batch Size under High Load. We make a key observation that the utility of lower accuracy $\text{Acc}(\phi_{\text{low}})$, higher batch sizes (B_{high}) configurations is higher than higher accuracy ($\text{Acc}(\phi_{\text{high}})$), lower batch size (B_{low}) configuration in pareto-subnets of SubNetAct. This is because the factor difference in accuracy of pareto-subnets (< 1) is less than the factor

differences of batch-sizes as seen in Fig. 13a i.e., $\frac{\text{Acc}(\phi_{\text{high}})}{\text{Acc}(\phi_{\text{low}})} \leq \frac{|B_{\text{high}}|}{|B_{\text{low}}|} \Rightarrow \text{Acc}(\phi_{\text{high}}) \cdot |B_{\text{low}}| \leq \text{Acc}(\phi_{\text{low}}) \cdot |B_{\text{high}}|$. Therefore, $\mathbb{U}(\phi_{\text{low}}, B_{\text{high}}, d_q) \geq \mathbb{U}(\phi_{\text{high}}, B_{\text{low}}, d_q)$ may hold true under high load, in cases where the most urgent query q in a batch of k queries ($q \in B_k$) can be served either by a) low accuracy model (ϕ_{min}) with batch size B_k or b) higher accuracy model (ϕ_{max}) on a subset of queries (say m , $q \in B_m$) with remaining queries ($B_k \setminus B_m$) missing the deadline due to high load. In such cases, the offline ILP will tend to option (a). SlackFit also tends to lower accuracy and higher batch size options under heavy load, as described in “SlackFit’s Behavior” (§4.2).

C. Offline ILP and SlackFit Prefer Higher Accuracy under Low Load. We make yet another observation from the latency profiles of sampled pareto-optimal subnets in Fig. 13a. For a batch size B , such that $B = B_1 + B_2$ where $B_1 > B_2$, the following holds true in many cases - $B_1 \cdot \text{Acc}(\phi_{\text{high}}) + B_2 \cdot \text{Acc}(\phi_{\text{low}}) > B \cdot \text{Acc}(\phi_{\text{mid}})$. Therefore, $\mathbb{U}(\phi_{\text{high}}, B_1, d_q) + \mathbb{U}(\phi_{\text{low}}, B_2, d(B_2)) \geq \mathbb{U}(\phi_{\text{mid}}, B, d_q)$, may hold true under low load, where the most urgent query q in batch B can be served by either a) mid accuracy model (ϕ_{mid}) with batch size B , or b) high accuracy model (ϕ_{high}) with larger-size batched partition B_1 ($q \in B_1$) with rest of the queries in batch B_2 served with the low accuracy model (ϕ_{low}) and meeting deadline $d(B_2)$. In such cases, ILP will tend to option (b) i.e., an option with higher average accuracy. SlackFit also tends to higher accuracy subnets under lower load, as described in §4.2.

5 SuperServe: System Architecture

SuperServe is a system that instantiates both SubNetAct mechanism and SlackFit policy. SuperServe’s architecture is illustrated in Fig. 7. The SuperServe client submits asynchronous RPC queries to the router with a deadline. These queries are enqueued to a global earliest-deadline-first (EDF) queue (❶). As soon as any worker becomes available, SuperServe’s fine-grained scheduler is invoked (❷). It decides on the query-batch (B) and the subnet (ϕ) which are then dispatched to the worker (❸). Upon receiving this query-batch, the worker that instantiates the supernet instantaneously actuates the chosen subnet in-place on the GPU using SubNetAct (❹), performs inference (❺), and returns predictions for the query-batch (❻). The router redirects these predictions back to the client (❼).

Router. The router runs fine-grained scheduler and interfaces with workers via RPCs. All queries are received, enqueued, and dequeued asynchronously in the router. It maintains pending queries in a global EDF queue, ordered by timestamps which denote query deadlines. The router invokes the scheduler whenever (a) a worker signals availability and (b) the EDF queue is not empty. It then sends query-batches to workers and also passes back the predictions to the clients.

Fine-grained Scheduler. The scheduler’s control decision is a batch-size and subnet ($\phi = (\mathbb{D}, \mathbb{E}, \mathbb{W})$). The scheduler provide pluggable APIs for different policy implementations.

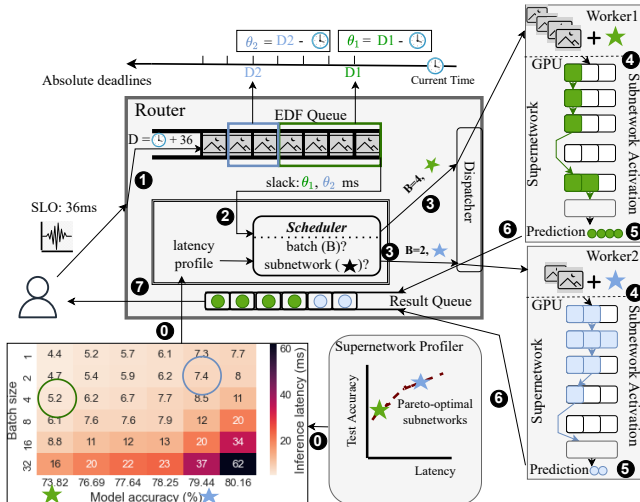


Fig. 7: SuperServe’s Architecture. SuperServe consists of a router, scheduler, workers and a supernet profiler. Clients submit queries with a specified latency constraint (SLO) asynchronously. ① - ⑦ represents the critical path of the query in SuperServe. The latency profile estimation is done a priori, off the critical path by the profiler.

SlackFit is one such policy implemented in the scheduler. All policies in scheduler leverage two key properties to make control decisions: (a) predictability of DNN inference latency, (b) fast actuation of SubNetAct on the query’s critical path.

Worker. The DNN worker employs the SubNetAct mechanism to host a supernet (R3). SubNetAct’s operators are implemented in TorchScript’s intermediate representation (IR) [14]. After receiving a query-batch and subnet (\mathbb{D} , \mathbb{E} , \mathbb{W}) from the router, the worker actuates the desired subnet inplace using SubNetAct. A forward pass on the actuated subnet produces predictions that are returned to the router. The router’s scheduler gets notified about worker availability on receiving the predictions.

Supernet Profiler. A supernet profiler is used when a supernet is submitted to SuperServe. This profiling completes a priori, before the workload begins, and off the critical path of the queries. The profiler first employs neural architecture search (NAS) [6] to find pareto-optimal subnetworks from the supernet for each latency target (key design choice of SlackFit §4.2). The latency profiling is done the pareto-optimal subnets obtained by NAS. This latency is a function of batch size and target worker GPU (latency profile in Fig. 7 on RTX2080Ti GPU), and the profiling process for the subnetworks is no different than the model profiling done for other existing models like ResNets [24], Wide-ResNets [58], ConvNeXt [35] etc.

6 Evaluation

We assess SuperServe’s end-to-end performance i.e., its ability to maximize SLO attainment (R1) and accuracy (R2)

under a variety of traffic conditions, including synthetic traces (§6.2) and real-world derived Microsoft Azure Functions trace (§6.3). SuperServe is resource-efficient (R3) due to the use of SubNetAct mechanism, already established in §3.1. We conclude with microbenchmarks (§6.4) that show SuperServe linearly scaling to 33,000 qps and providing transparent fault tolerance.

6.1 Experimental Setup

Success metrics. *SLO attainment* is defined as the fraction of the queries that complete within the latency deadline (R1). The *mean serving accuracy* is calculated for the queries that satisfy the SLO and is the average of models’ profiled accuracy that were used to serve the queries (R2).

Traces. We evaluate SuperServe on three sets of traces: bursty, time-varying, and real-world. Bursty and time-varying traces are synthetic, similar to those used in InferLine [10]. We construct the *bursty traces* by starting with a base arrival with mean ingest rate λ_b (with $CV^2 = 0$) and add a variant arrival trace with mean ingest rate λ_v drawing inter-arrival times from a gamma distribution (Fig. 12a). We vary λ_b , λ_v and CV^2 . *Time-varying* traces differ from bursty by varying the mean ingest throughput over time. We change the mean from $\mu = 1/\lambda_1$ to $\mu = 1/\lambda_2$ at rate $\tau q/s^2$ with a fixed CV_a^2 . Higher ingest acceleration $\tau q/s^2$ corresponds to faster change from λ_1 to λ_2 . All synthetic trace generation is seeded. Lastly, we use a MAF trace [45] for evaluation on a real-world workload.

Baselines. We compare SuperServe with the single model serving systems that don’t perform accuracy trade-offs (and the models are manually selected by users, non-automated serving systems in §7). These systems are represented as Clipper+ baseline and include systems like Clipper [11], Clockwork [22], and TF-serving [37]. Clipper+ is manually configured to serve six different accuracy points (subnets) that uniformly span the supernet’s accuracy range and result in its six different versions. We also compare SuperServe with INFaaS and note that INFaaS is designed to “pick the most cost-efficient model that meets the [specified] accuracy constraint” [15,42,43]. However, in the presence of unpredictable, bursty request rates, the choice of the model accuracy to serve in order to meet the SLO requirements is unknown. Since, unlike SuperServe, INFaaS does not automatically discover the accuracy of the model to serve under unpredictable request rates and instead requires queries to be hand-annotated with accuracy thresholds, we choose to run INFaaS with no accuracy thresholds provided (§6.2.1, §6.2.2). In such a scenario, INFaaS reduces to serving the most cost-efficient model (which is the model with the minimum accuracy). We confirmed this behavior with the INFaaS authors, who agree that “[our] representation of INFaaS as a baseline that always chooses the same model is correct in the absence of an accuracy threshold, or a fixed (never changing) accuracy threshold.” [15].

Subnet-Profiling. We use the supernet trained on ImageNet [12] dataset released by [6] and enable SubNetAct in it. We extract pareto-subnets (Φ_{pareto}) by running NAS (publicly released by [6]) on trained supernet. The pareto-subnets in the supernet span 0.9 – 7.5 GFLOPs range and an accuracy range of 73 – 80%. Pareto-subnets are profiled with varied batch sizes on NVIDIA RTX2080Ti GPU.

Test bed. SuperServe is implemented in C++ (17,500 lines of code). gRPC [20] is used for communication between a client, the router and workers. The experiments use 8 RTX2080Ti GPUs and 24 CPU cores. Each worker uses one GPU.

6.2 End-to-End: Synthetic

We aim to answer the following questions, whether SuperServe (a) *automatically* serves queries using appropriate models (accuracy) for different traces (**R2**), (b) achieves a better trade-off w.r.t. the success metrics (**R1-R2**), (c) withstands sharp bursts while maintaining high SLO attainment (**R1**) and (d) *instantaneously* changes system capacity to serve traces where mean ingest rate changes over time. To answer these questions, we evaluate SuperServe on the bursty and time-varying traces (§6.1).

6.2.1 Baseline comparison with burstiness

Fig. 8 compares SuperServe with the baselines over a range of traces increasing mean ingest rate λ_v across and CV_a^2 down. All traces are configured with 36ms SLO. Achieving high SLO attainment (**R1**) and high mean serving accuracy (**R2**) is desirable, which implies the *best trade-off is in the top-right corner of the graph*. We demonstrate that no single choice of a model is *sufficient* for different mean arrival rates and CV_a^2 . For instance, the SLO attainment of Clipper⁺(76.69) decreases as the CV_a^2 increases for $\lambda_v = 5550$ (row 3). Similarly, the SLO attainment of Clipper⁺(78.25) decreases with increase in λ_v for $CV_a^2 = 2$ (column 1). We draw the following takeaways: **(1)** SuperServe achieves a significantly better trade-off between SLO attainment and accuracy (**R1-R2**) than the baselines (Clipper⁺ and InFaaS). It is 4.33% more accurate than the baselines at an SLO attainment level of 0.9999 and 2.06x higher SLO attainment at the same accuracy level. SuperServe is consistently at the top-right corner in Fig. 8 across all the traces. **(2)** SlackFit *automatically* selects appropriate models for sustaining different traffic conditions. As λ_v increases, SuperServe reduces serving accuracy while maintaining high SLO attainment (columns).

Note that, across all the traces, InFaaS achieves an optimal SLO attainment but with a significantly smaller mean serving accuracy (by up to 4.33%) than SuperServe. InFaaS policy serves the min-cost (and hence min accuracy) model for the trace without accuracy constraints. Whereas, SuperServe achieves a better trade-off between the success metrics because (a) SubNetAct allows in place activation of dif-

ferent subnetworks *without* affecting SLO attainment (**R1**); (b) SlackFit opportunistically selects higher accuracy models based on query’s slack (**R2**). Also, the difference between SuperServe and Clipper⁺ narrows w.r.t. accuracy as CV_a^2 increases. This is because SlackFit switches to lower accuracy models more frequently with burstier traffic. This system dynamics is detailed in §A.2.

6.2.2 Baseline comparison with arrival acceleration

Fig. 9 evaluates SuperServe performance at different levels of arrival rate change (i.e., arrival *acceleration*). Traces start at λ_1 and increase to λ_2 with acceleration τ . Traces fix $\lambda_1 = 2500qps$ and $CV_a^2 = 8$ but change λ_2 and acceleration τ .

The τ and λ_2 are chosen to demonstrate that single, pre-configured model choices are inadequate to sustain different rates of arrival (mean λ) and acceleration (τ). Clipper⁺(79.44) starts diverging as τ increases (λ_2 is 6800 *qps* (row 2)). Similarly, Clipper⁺(79.44) starts diverging with increase in λ_2 ($\tau = 250 q/s^2$ (column 1)). The key takeaways from this experiment are as follows:

- SuperServe *rapidly* scales system capacity and achieves a high SLO attainment (0.991-1.0) even with high values of τ (5000 *q/s^2*). The experiment demonstrates two key properties of SuperServe— (a) the *actuation delay* in SuperServe is indeed negligible, (b) the lower *actuation delay* helps achieve higher SLO attainments for time-varying traces (**R1**). SuperServe empirically demonstrates “agile elasticity” (§2.2), and withstands high acceleration in arrival rate (τ).
- SlackFit *dynamically* adjusts the serving accuracy over time (**R2**) and achieves a better trade-off between success metrics (**R1-R2**). When the mean ingest throughput is low (λ_1), SuperServe uses higher accuracy models. It quickly switches to lower accuracy models when mean arrival rate is high (λ_2), as evident in system dynamics Fig. 12b.

Fig. 9 experiments exhibit interesting trends. As the τ increases, the gap between SuperServe and Clipper⁺ w.r.t. mean serving accuracy narrows. This is because SlackFit selects smaller accuracy sooner with the increase in τ . Lower τ values give enough time to SuperServe to serve intermediate mean arrival rates with higher accuracy models while gradually moving to lower accuracy models as mean ingest rate increases to λ_2 *qps*. Whereas, InFaaS continues to serve min accuracy model for all traces as its policy doesn’t maximize accuracy by design.

6.3 End-to-End: Real Workloads

We investigate if: (a) SlackFit is capable of achieving a better trade-off between SLO attainment and mean serving accuracy on real workloads (**R1-R2**), and (b) SubNetAct contributes to serve highly unpredictable workloads at high SLO attainment.

We use the MAF trace [45] to evaluate SuperServe (similar to Clockwork [22]). The trace is collected on Microsoft’s

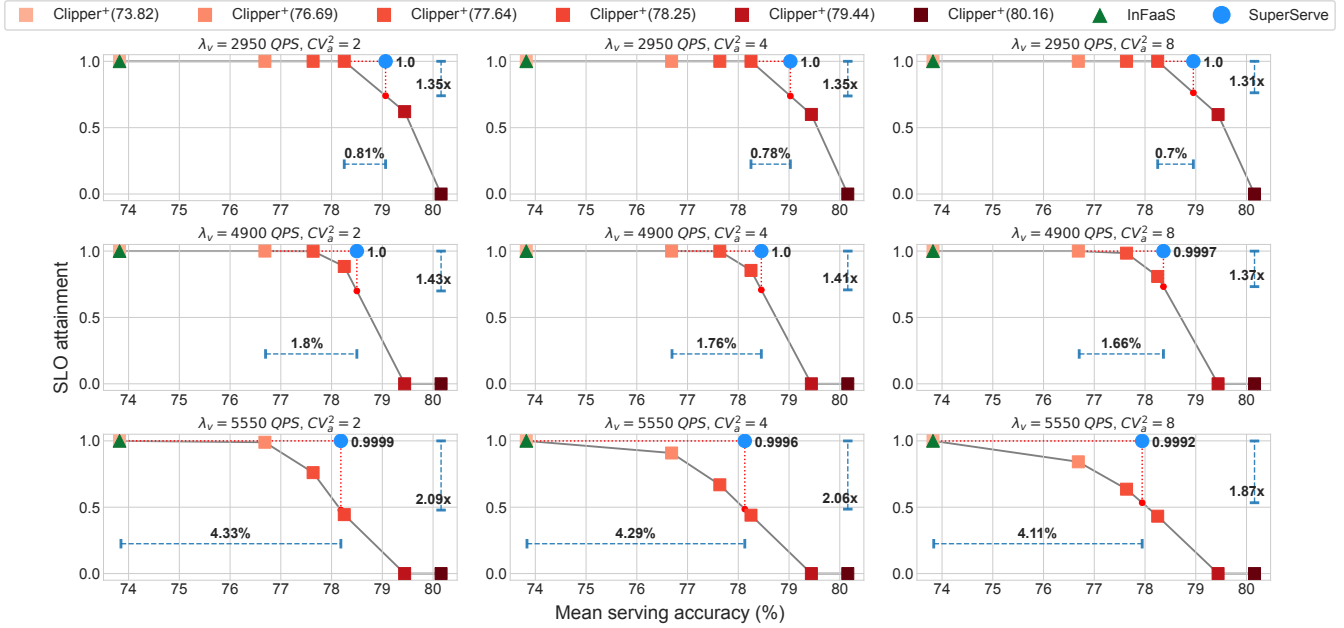


Fig. 8: SuperServe with variable burstiness. SuperServe outperforms Clipper⁺ and INFaaS baselines by finding better tradeoffs and consistently achieving > 0.999 SLO attainment on bursty traces. Variable ingest rate $\lambda_v = \{2950, 4900, 5550\}$ q/s increases vertically (down). $CV_a^2 = \{2, 4, 8\}$ increases horizontally (across). SuperServe achieves a better trade-off in SLO attainment (y-axis) and mean serving accuracy (x-axis) in all cases. SuperServe consistently achieves high SLO attainment > 0.999.

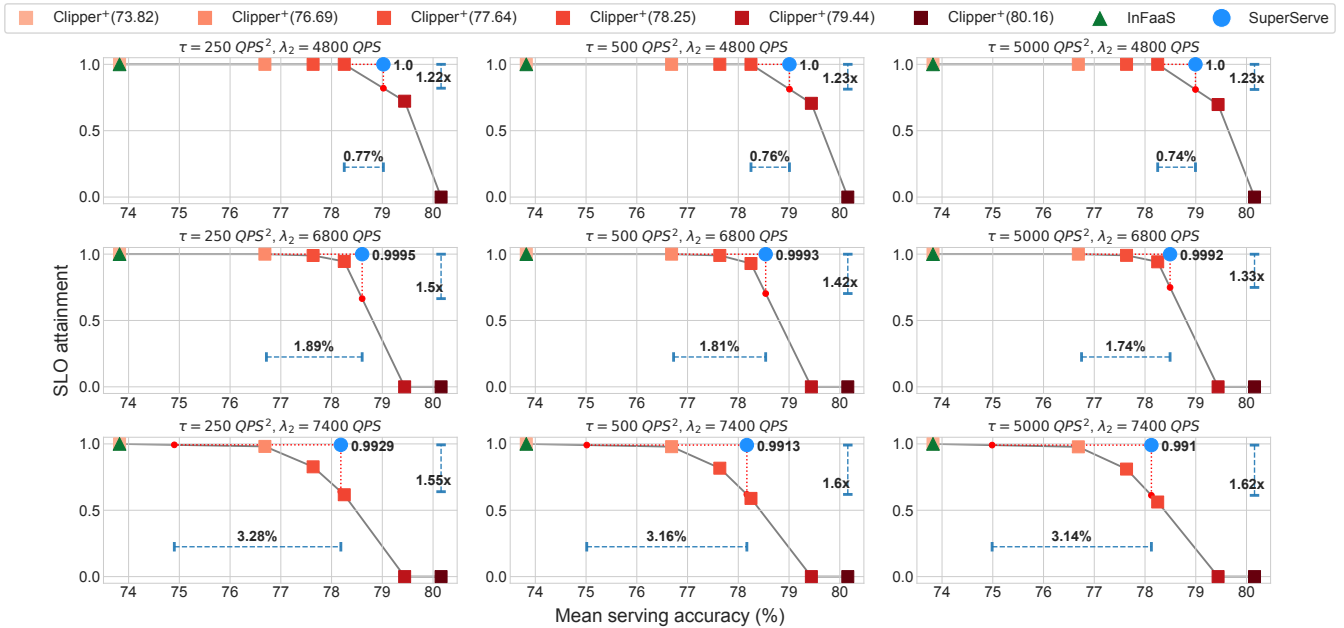
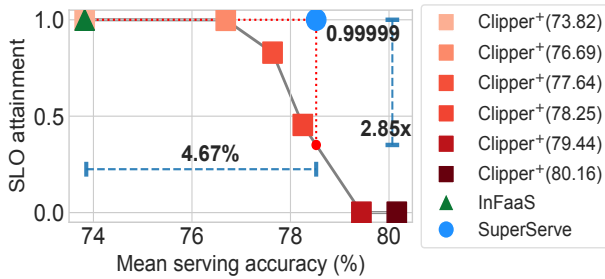


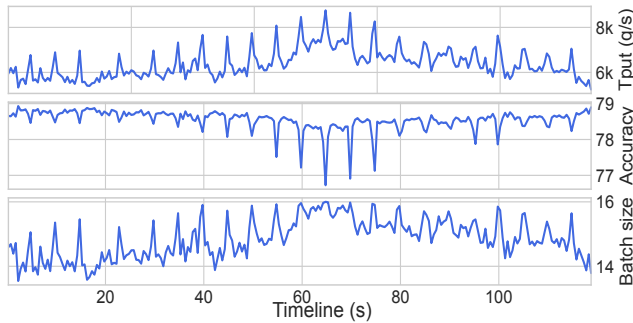
Fig. 9: SuperServe with arrival acceleration. SuperServe outperforms Clipper⁺ and INFaaS baselines by finding better tradeoffs on time varying traces. Mean ingest rate accelerates from λ_1 to λ_2 q/s with τ q/s^2 . $\tau = \{250, 500, 5000\}$ increases horizontally (across), while $\lambda_2 = \{4800, 6800, 7800\}$ increases vertically (down) with $\lambda_1 = 2500$ q/s and $CV_a^2 = 8$ staying constant. SuperServe finds a better trade-off in SLO attainment (y-axis) and mean serving accuracy (x-axis).

serverless platform and serves as a reasonable workload to evaluate SuperServe as serverless ML inference is an active

research area [28, 55]. It consists of number of invocations made for each function per minute and contains nearly 46,000



(a) SuperServe achieves best tradeoffs w.r.t. SLO attainment and accuracy on a real trace.



(b) SuperServe System Dynamics

Fig. 10: SuperServe on Real World Trace. SuperServe on Microsoft Azure Functions (MAF) [45] trace. (a) SuperServe is compared with Clipper⁺ and InFaaS baselines, reaching 4.67% higher accuracy at same SLO attainment and 2.85x higher SLO attainment at same accuracy than any fixed accuracy point that can be served by InFaaS (in the absence of accuracy constraints) and Clipper⁺. (b) System dynamics w.r.t. batch size and subnet activation control decisions over time in response to ingest rate in the top graph.

different function workloads that are bursty, periodic, and fluctuate over time. We use 32,700 function workloads from the MAF trace, resulting in a mean arrival rate of 6400 qps. The 24 hour long trace is shrunk to 120 seconds using *shape-preserving* transformations to match our testbed.

Result. Fig. 10a compares SuperServe with Clipper⁺ and InFaaS on the real-world MAF trace. SuperServe achieves an SLO attainment (**R1**) of 0.99999 (five ‘9’s). Compared to Clipper⁺ and InFaaS, SuperServe is 4.65% more accurate (**R2**) at the same level of SLO attainment. It also achieves 2.85x factor improvement in SLO attainment at the same mean serving accuracy. Moreover, Clipper⁺(79.44, 80.16) diverges on the MAF trace.

System Dynamics. Fig. 10b shows the ingest throughput (qps), serving accuracy and batch size control decisions (made by SlackFit) for the MAF trace. As seen in the figure, the trace contains periodic short-interval spikes that reach upto 8750 qps, demonstrating the agility of the system. SlackFit selects both smaller accuracy model and higher batch size during the load spikes to meet the deadline (**R1**). SlackFit makes such control decisions because it uses query’s slack as a signal to

maximize batch size. As the query slack decreases, it selects maximum batch size control parameters in the lower latency buckets. Furthermore, these control decisions increase the system capacity instantly through SubNetAct. Lastly, SlackFit serves higher accuracy models when the ingest rate is low and hence, achieves better mean serving accuracy (**R2**).

6.4 Microbenchmarks

Fault Tolerance. SubNetAct mechanism provides an additional advantage of transparent fault tolerance. We run SuperServe with 100% capacity (8 workers) with a bursty traffic trace ($\lambda = 3500$ qps, $CV_a^2 = 2$) for 60 seconds and gradually kill a worker every 12 seconds to simulate faults. SuperServe shows resilience to decreases in system throughput capacity to as low as 50% by maintaining SLO attainment as high as 0.999 for the unchanging trace as it leverages subnetwork activation to serve lower accuracy models automatically. Similar methodology was used in [53]. Fig. 11a shows SLO attainment as a function of time (along with other system dynamics). As the faults occur (workers killed, dotted red lines), SuperServe *automatically* transitions to lower accuracy models to maintain high SLO attainment. We attribute SuperServe’s fault tolerance to (a) a wide-dynamic throughput range afforded by SubNetAct (Fig. 5c) that allows SuperServe to serve the workload even with 50% capacity, and (b) SubNetAct’s low actuation delay that provides *agility* to rapidly increase system-capacity (during faults) without sacrificing SLO attainment (**R1**).

Scalability. We assess if SuperServe reaches high SLO attainment at scale. To show this, we scale the number of workers and observe the maximum throughput SuperServe sustains to reach SLO attainment of 0.999. We serve Resnet-18 [24] across all the workers with clients providing a batch of 8 images³. Scalability experiments are conducted with $CV_a^2 = 0$. Fig. 11b shows sustained ingest throughput with the increase in workers. In this experiment SuperServe achieves an SLO attainment of 0.999 while reaching throughputs as high as ≈ 33000 qps.

Policy Space Exploration. We compare different policies implemented in SuperServe (Fig. 11c). We show that SlackFit achieves the best tradeoff w.r.t. our success metrics compared to both MaxAcc (greedily maximizes accuracy) and MaxBatch (greedily maximizes throughput) as CV_a^2 is varied. Details of the policies and the experiment are in §A.5.

7 Related Work

We build on recent DNN supernet training progress, which is complementary to this work. [6, 44] train supernets for image classification vision tasks [?]. Dynabert [25] supernet

³we don’t perform adaptive batching for this experiment

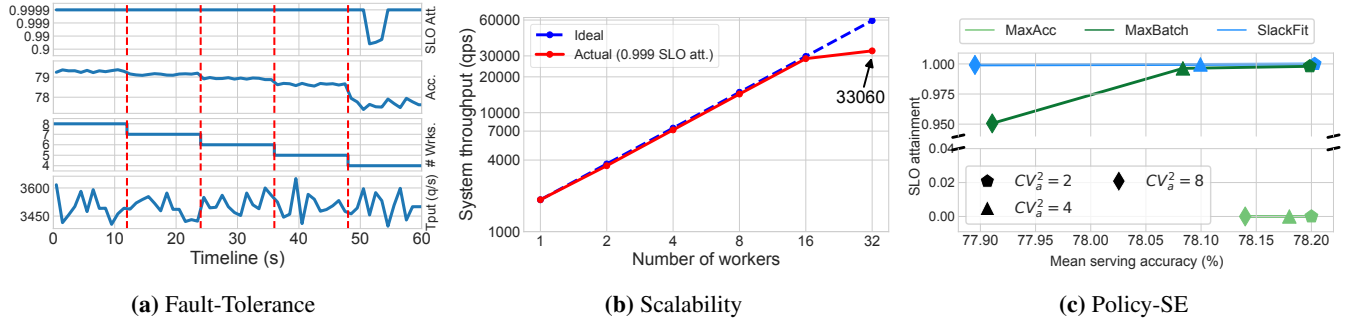


Fig. 11: SuperServe’s Micro-benchmarks. (a) SuperServe resiliency to faults. SuperServe maintains high SLO attainment in the system by dynamically adjusting served accuracy as workers drop out over time. The trace stays statistically the same ($\lambda = 3500$ qps, $CV_a^2 = 2$ (last row)). (b) SuperServe scales linearly with the number of workers, achieving up to 33000 qps (orders of magnitude higher than published SotA systems) while maintaining high .999 SLO attainment. (c) SlackFit finds the best tradeoff on the SLO attainment/accuracy maximization continuum automatically (§6.4).

supports NLP tasks trained on GLUE [52], including textual entailment, question answering and sentiment analysis.

Model serving systems can be broadly divided into two categories — a) Non-Automated, and b) Automated. *Non-automated serving system* expect application developers to provide the prediction models and make explicit choices in the accuracy-latency trade-off space. This category includes TensorFlow serving [37], Clipper [11], InferLine [10], SageMaker [30], Triton [36], Shepherd [59] and Clockwork [22]. TensorFlow Serving serves the models trained in TensorFlow framework while Clipper and Triton support models trained from multiple frameworks. Triton optimizes models for GPU serving. Clockwork guarantees predictable tail latency for DNN inference by designing a predictable system bottom up and making cross-stack design decisions explicitly for worst case predictability. Inferline provides support for provisioning inference pipelines that consist of multiple models, but the models are still hard coded in the pipeline vertices. However, all the prior works in this category are complementary to SuperServe. For instance, SuperServe’s workers can be made more predictable by consolidating choices like Clockwork. Inferline’s autoscaling policy can be used on top of SuperServe. The max-provisioning ratio of the smallest subnetwork in SuperServe can be calculated to construct traffic envelopes for Inferline’s high frequency tuner. The workers can then be scaled up if the ingest throughput cannot be served by the smallest subnetwork of the supernet.

In contrast, *automated serving systems* [42, 60] provide a mechanism for switching between available latency/accuracy points and automate the navigation of the accuracy-latency trade-off space with a policy, resulting in automatic DNN selection at runtime. However, both [42] and [60] use state-of-the-art DNNs (e.g., ResNets, MobileNets) and rely on model loading mechanism instead of the supernet, which offers better pareto-optimality and orders of magnitude faster model switching enabled via proposed SubNetAct. Fundamentally, these state of the art mechanisms implicitly bias their policies

to avoid model switching, which clearly limits the ability of the system to respond to unpredictable trace and query complexity dynamics in an agile fashion. InFaaS’s DNN switching policy is biased towards selecting the least accurate DNNs that satisfy accuracy constraints, as the goal of the stated goal of the system is to satisfy constraints instead of treating accuracy as an optimization objective. Model-Switching [60] switches between CPU models only. Thus, it cleverly never incurs the overhead of GPU model loading faced by other systems such as InFaaS and Clockwork. SuperServe supports GPU model serving via subnetwork activation, addressing the model switching overhead through its proposed SubNetAct.

Training Supernets. Supernet (as a concept) and its training was first proposed by OFA [6]. The subnetworks trained as a part of training the supernet are shown to offer a better accuracy-latency trade-off than existing models like EfficientNets [49], ResNets [24], MobileNets [26] and SlimmableNets [57]. Furthermore, there is a surge of recent works that propose improvements to the supernet training such as CompOFA [44], and BigNAS [56]. For instance, CompOFA makes the training of Supernets faster and more accurate by training a fewer number of subnetworks simultaneously. While BigNAS trains the supernet in a one-shot fashion with a wider range of subnetworks. Dynabert [25] trains a supernet based on transformer neural network architecture for text datasets. It varies the depth and hidden dimensions in BERT-like models. AutoFormer [9] is another technique that trains supernets derived from vision transformers. The subnetworks extracted from AutoFormer’s supernet surpass state-of-the-art vision transformers like ViT [13] and DeiT [50]. NasViT [19] trains the supernet for semantic segmentation tasks and achieves a better trade-off between accuracy and latency at fewer FLOPs. SuperServe provides system support for serving Supernets trained using any existing technique. We believe that Supernets are an emerging phenomenon, and system support for serving them is the need of the hour.

8 Conclusion

We describe a novel mechanism SubNetAct that carefully inserts specialized control-flow and slicing operators into SuperNets to enable a resource-efficient, fine-grained navigation of the latency-accuracy tradeoff space. SubNetAct unlocks the design space of fine-grained, reactive scheduling policies. We explore the design of one such simple, yet effective greedy heuristic-based scheduling policy SlackFit. We instantiate SubNetAct and SlackFit in SuperServe, and extensively evaluate it on real-world workloads. SuperServe achieves 4.67% better accuracy at the same level of SLO attainment or 2.85x better SLO attainment at the same level of serving accuracy compared to state-of-the-art inference-serving systems.

References

- [1] Accelerate ai development with google cloud tpus. <https://cloud.google.com/tpu>.
- [2] Aws inferentia. <https://aws.amazon.com/machine-learning/inferentia/>.
- [3] Waleed Ali, Sherif Abdelkarim, Mahmoud Zidan, Mohamed Zahran, and Ahmad El Sallab. Yolo3d: End-to-end real-time 3d oriented object bounding box detection from lidar point cloud. In *Proceedings of the European Conference on Computer Vision (ECCV) Workshops*, pages 0–0, 2018.
- [4] Ganesh Ananthanarayanan, Paramvir Bahl, Peter Bodík, Krishna Chintalapudi, Matthai Philipose, Lenin Ravindranath, and Sudipta Sinha. Real-time video analytics: The killer app for edge computing. *computer*, 50(10):58–67, 2017.
- [5] Bowen Baker, Otkrist Gupta, Nikhil Naik, and Ramesh Raskar. Designing neural network architectures using reinforcement learning. *arXiv preprint arXiv:1611.02167*, 2016.
- [6] Han Cai, Chuang Gan, Tianzhe Wang, Zhekai Zhang, and Song Han. Once-for-all: Train one network and specialize it for efficient deployment. In *International Conference on Learning Representations*, 2020.
- [7] Han Cai, Ligeng Zhu, and Song Han. Proxylessnas: Direct neural architecture search on target task and hardware. *arXiv preprint arXiv:1812.00332*, 2018.
- [8] Liang-Chieh Chen, George Papandreou, Florian Schroff, and Hartwig Adam. Rethinking atrous convolution for semantic image segmentation. *arXiv preprint arXiv:1706.05587*, 2017.
- [9] Minghao Chen, Houwen Peng, Jianlong Fu, and Haibin Ling. Autoformer: Searching transformers for visual recognition. In *Proceedings of the IEEE/CVF international conference on computer vision*, pages 12270–12280, 2021.
- [10] Daniel Crankshaw, Gur-Eyal Sela, Corey Zumar, Xiangxi Mo, Joseph E. Gonzalez, Ion Stoica, and Alexey Tumanov. Inferline: ML inference pipeline composition framework. *CoRR*, abs/1812.01776, 2018.
- [11] Daniel Crankshaw, Xin Wang, Guilio Zhou, Michael J Franklin, Joseph E Gonzalez, and Ion Stoica. Clipper: A {Low-Latency} online prediction serving system. In *14th USENIX Symposium on Networked Systems Design and Implementation (NSDI 17)*, pages 613–627, 2017.

- [12] Jia Deng, Wei Dong, Richard Socher, Li-Jia Li, Kai Li, and Li Fei-Fei. Imagenet: A large-scale hierarchical image database. In *2009 IEEE conference on computer vision and pattern recognition*, pages 248–255. Ieee, 2009.
- [13] Alexey Dosovitskiy, Lucas Beyer, Alexander Kolesnikov, Dirk Weissenborn, Xiaohua Zhai, Thomas Unterthiner, Mostafa Dehghani, Matthias Minderer, Georg Heigold, Sylvain Gelly, et al. An image is worth 16x16 words: Transformers for image recognition at scale. *arXiv preprint arXiv:2010.11929*, 2020.
- [14] Facebook. Torchscript, 2022.
- [15] Romero Francisco, Qian Li, and Christos Kozyrakis. Personal Communication, December 2022.
- [16] Shen Gao, Xiuying Chen, Piji Li, Zhaochun Ren, Lidong Bing, Dongyan Zhao, and Rui Yan. Abstractive text summarization by incorporating reader comments. In *Proceedings of the AAAI Conference on Artificial Intelligence*, volume 33, pages 6399–6406, 2019.
- [17] Ionel Gog, Sukrit Kalra, Peter Schafhalter, Joseph E Gonzalez, and Ion Stoica. D3: a dynamic deadline-driven approach for building autonomous vehicles. In *Proceedings of the Seventeenth European Conference on Computer Systems*, pages 453–471, 2022.
- [18] Ionel Gog, Sukrit Kalra, Peter Schafhalter, Matthew A Wright, Joseph E Gonzalez, and Ion Stoica. Pylot: A modular platform for exploring latency-accuracy trade-offs in autonomous vehicles. In *2021 IEEE International Conference on Robotics and Automation (ICRA)*, pages 8806–8813. IEEE, 2021.
- [19] Chengyue Gong, Dilin Wang, Meng Li, Xinlei Chen, Zhicheng Yan, Yuandong Tian, Vikas Chandra, et al. Nasvit: Neural architecture search for efficient vision transformers with gradient conflict aware supernet training. In *International Conference on Learning Representations*, 2021.
- [20] Google. grpc, 2022.
- [21] Arpan Gujarati, Sameh Elnikety, Yuxiong He, Kathryn S. McKinley, and Björn B. Brandenburg. Swayam: Distributed autoscaling to meet slas of machine learning inference services with resource efficiency. In *Proceedings of the 18th ACM/IFIP/USENIX Middleware Conference*, Middleware '17, page 109–120, New York, NY, USA, 2017. Association for Computing Machinery.
- [22] Arpan Gujarati, Reza Karimi, Safya Alzayat, Wei Hao, Antoine Kaufmann, Ymir Vigfusson, and Jonathan Mace. Serving DNNs like clockwork: Performance predictability from the bottom up. In *14th USENIX Symposium on Operating Systems Design and Implementation (OSDI 20)*, pages 443–462. USENIX Association, November 2020.
- [23] Kim Hazelwood, Sarah Bird, David Brooks, Soumith Chintala, Utku Diril, Dmytro Dzhulgakov, Mohamed Fawzy, Bill Jia, Yangqing Jia, Aditya Kalro, et al. Applied machine learning at facebook: A datacenter infrastructure perspective. In *2018 IEEE International Symposium on High Performance Computer Architecture (HPCA)*, pages 620–629. IEEE, 2018.
- [24] Kaiming He, Xiangyu Zhang, Shaoqing Ren, and Jian Sun. Deep residual learning for image recognition. In *Proceedings of the IEEE conference on computer vision and pattern recognition*, pages 770–778, 2016.
- [25] Lu Hou, Zhiqi Huang, Lifeng Shang, Xin Jiang, Xiao Chen, and Qun Liu. Dynabert: Dynamic bert with adaptive width and depth. In H. Larochelle, M. Ranzato, R. Hadsell, M.F. Balcan, and H. Lin, editors, *Advances in Neural Information Processing Systems*, volume 33, pages 9782–9793. Curran Associates, Inc., 2020.
- [26] Andrew Howard, Mark Sandler, Grace Chu, Liang-Chieh Chen, Bo Chen, Mingxing Tan, Weijun Wang, Yukun Zhu, Ruoming Pang, Vijay Vasudevan, et al. Searching for mobilenetv3. In *Proceedings of the IEEE/CVF International Conference on Computer Vision*, pages 1314–1324, 2019.
- [27] Sergey Ioffe and Christian Szegedy. Batch normalization: Accelerating deep network training by reducing internal covariate shift. In *International conference on machine learning*, pages 448–456. PMLR, 2015.
- [28] Vatche Ishakian, Vinod Muthusamy, and Aleksander Slominski. Serving deep learning models in a serverless platform. *CoRR*, abs/1710.08460, 2017.
- [29] Haoming Jiang, Pengcheng He, Weizhu Chen, Xiaodong Liu, Jianfeng Gao, and Tuo Zhao. SMART: Robust and efficient fine-tuning for pre-trained natural language models through principled regularized optimization. In *Proceedings of the 58th Annual Meeting of the Association for Computational Linguistics*, pages 2177–2190, Online, July 2020. Association for Computational Linguistics.
- [30] Ameet V Joshi. Amazon’s machine learning toolkit: Sagemaker. In *Machine Learning and Artificial Intelligence*, pages 233–243. Springer, 2020.
- [31] Sangeetha Abdu Jyothi, Carlo Curino, Ishai Menache, Shraavan Matthur Narayanamurthy, Alexey Tumanov, Jonathan Yaniv, Ruslan Mavlyutov, Inigo Goiri, Subru

- Krishnan, Janardhan Kulkarni, et al. Morpheus: towards automated {SLOs} for enterprise clusters. In *12th USENIX Symposium on Operating Systems Design and Implementation (OSDI 16)*, pages 117–134, 2016.
- [32] Zhuohan Li, Lianmin Zheng, Yinmin Zhong, Vincent Liu, Ying Sheng, Xin Jin, Yanping Huang, Zhifeng Chen, Hao Zhang, Joseph E Gonzalez, et al. {AlpaServe}: Statistical multiplexing with model parallelism for deep learning serving. In *17th USENIX Symposium on Operating Systems Design and Implementation (OSDI 23)*, pages 663–679, 2023.
- [33] Shih-Chieh Lin, Yunqi Zhang, Chang-Hong Hsu, Matt Skach, Md E Haque, Lingjia Tang, and Jason Mars. The architectural implications of autonomous driving: Constraints and acceleration. In *Proceedings of the Twenty-Third International Conference on Architectural Support for Programming Languages and Operating Systems*, pages 751–766, 2018.
- [34] Hanxiao Liu, Karen Simonyan, and Yiming Yang. Darts: Differentiable architecture search. *arXiv preprint arXiv:1806.09055*, 2018.
- [35] Zhuang Liu, Hanzi Mao, Chao-Yuan Wu, Christoph Feichtenhofer, Trevor Darrell, and Saining Xie. A convnet for the 2020s. In *Proceedings of the IEEE/CVF conference on computer vision and pattern recognition*, pages 11976–11986, 2022.
- [36] Nvidia. Triton inference system, 2020.
- [37] Christopher Olston, Noah Fiedel, Kiril Gorovoy, Jeremiah Harmsen, Li Lao, Fangwei Li, Vinu Rajashekhar, Sukriti Ramesh, and Jordan Soyke. Tensorflow-serving: Flexible, high-performance ml serving. *arXiv preprint arXiv:1712.06139*, 2017.
- [38] Kalin Ovtcharov, Olatunji Ruwase, Joo-Young Kim, Jeremy Fowers, Karin Strauss, and Eric S Chung. Accelerating deep convolutional neural networks using specialized hardware. *Microsoft Research Whitepaper*, 2(11):1–4, 2015.
- [39] Arthi Padmanabhan, Neil Agarwal, Anand Iyer, Ganesh Ananthanarayanan, Yuanhao Shu, Nikolaos Karianakis, Guoqing Harry Xu, and Ravi Netravali. Gemel: Model merging for {Memory-Efficient}, {Real-Time} video analytics at the edge. In *20th USENIX Symposium on Networked Systems Design and Implementation (NSDI 23)*, pages 973–994, 2023.
- [40] Christos H Papadimitriou and Kenneth Steiglitz. *Combinatorial optimization: algorithms and complexity*. Courier Corporation, 1998.
- [41] Jongsoo Park, Maxim Naumov, Protonu Basu, Summer Deng, Aravind Kalaiah, Daya Khudia, James Law, Parth Malani, Andrey Malevich, Satish Nadathur, et al. Deep learning inference in facebook data centers: Characterization, performance optimizations and hardware implications. *arXiv preprint arXiv:1811.09886*, 2018.
- [42] Francisco Romero, Qian Li, Neeraja J Yadwadkar, and Christos Kozyrakis. {INFaaS}: Automated model-less inference serving. In *2021 USENIX Annual Technical Conference (USENIX ATC 21)*, pages 397–411, 2021.
- [43] Francisco Romero, Qian Li, Neeraja J Yadwadkar, and Christos Kozyrakis. Infaas policy’s decisions with respect to accuracy constraints, 2022.
- [44] Manas Sahni, Shreya Varshini, Alind Khare, and Alexey Tumanov. Comp{ofa} – compound once-for-all networks for faster multi-platform deployment. In *International Conference on Learning Representations*, 2021.
- [45] Mohammad Shahrhad, Rodrigo Fonseca, Íñigo Goiri, Gohar Chaudhry, Paul Batum, Jason Cooke, Eduardo Laureano, Colby Tresness, Mark Russinovich, and Ricardo Bianchini. Serverless in the wild: Characterizing and optimizing the serverless workload at a large cloud provider. In *2020 USENIX Annual Technical Conference (USENIX ATC 20)*, pages 205–218, 2020.
- [46] Jonathan Soifer, Jason Li, Mingqin Li, Jeffrey Zhu, Yingnan Li, Yuxiong He, Elton Zheng, Adi Oltean, Maya Mosyak, Chris Barnes, et al. Deep learning inference service at microsoft. In *2019 USENIX Conference on Operational Machine Learning (OpML 19)*, pages 15–17, 2019.
- [47] Martin Sundermeyer, Ralf Schlüter, and Hermann Ney. Lstm neural networks for language modeling. In *Thirteenth annual conference of the international speech communication association*, 2012.
- [48] Mingxing Tan, Bo Chen, Ruoming Pang, Vijay Vasudevan, Mark Sandler, Andrew Howard, and Quoc V Le. Mnasnet: Platform-aware neural architecture search for mobile. In *Proceedings of the IEEE Conference on Computer Vision and Pattern Recognition*, pages 2820–2828, 2019.
- [49] Mingxing Tan and Quoc Le. Efficientnet: Rethinking model scaling for convolutional neural networks. In *International conference on machine learning*, pages 6105–6114. PMLR, 2019.
- [50] Hugo Touvron, Matthieu Cord, Matthijs Douze, Francisco Massa, Alexandre Sablayrolles, and Hervé Jégou. Training data-efficient image transformers & distillation through attention. In *International conference on machine learning*, pages 10347–10357. PMLR, 2021.

- [51] Prahlad Venkatapuram, Zhao Wang, and Chandra Mallipedi. Custom silicon at facebook: A datacenter infrastructure perspective on video transcoding and machine learning. In *2020 IEEE International Electron Devices Meeting (IEDM)*, pages 9–7. IEEE, 2020.
- [52] Alex Wang, Amanpreet Singh, Julian Michael, Felix Hill, Omer Levy, and Samuel R Bowman. Glue: A multi-task benchmark and analysis platform for natural language understanding. *arXiv preprint arXiv:1804.07461*, 2018.
- [53] Stephanie Wang, John Liagouris, Robert Nishihara, Philipp Moritz, Ujval Misra, Alexey Tumanov, and Ion Stoica. Lineage stash: fault tolerance off the critical path. In *Proceedings of the 27th ACM Symposium on Operating Systems Principles*, pages 338–352, 2019.
- [54] Carole-Jean Wu, David Brooks, Kevin Chen, Douglas Chen, Sy Choudhury, Marat Dukhan, Kim Hazelwood, Eldad Isaac, Yangqing Jia, Bill Jia, et al. Machine learning at facebook: Understanding inference at the edge. In *2019 IEEE international symposium on high performance computer architecture (HPCA)*, pages 331–344. IEEE, 2019.
- [55] Yanan Yang, Laiping Zhao, Yiming Li, Huanyu Zhang, Jie Li, Mingyang Zhao, Xingzhen Chen, and Keqiu Li. Inflex: A native serverless system for low-latency, high-throughput inference. In *Proceedings of the 27th ACM International Conference on Architectural Support for Programming Languages and Operating Systems, ASPLOS '22*, page 768–781, New York, NY, USA, 2022. Association for Computing Machinery.
- [56] Jiahui Yu, Pengchong Jin, Hanxiao Liu, Gabriel Bender, Pieter-Jan Kindermans, Mingxing Tan, Thomas Huang, Xiaodan Song, Ruoming Pang, and Quoc Le. Bignas: Scaling up neural architecture search with big single-stage models. In Andrea Vedaldi, Horst Bischof, Thomas Brox, and Jan-Michael Frahm, editors, *Computer Vision – ECCV 2020*, pages 702–717, Cham, 2020. Springer International Publishing.
- [57] Jiahui Yu, Linjie Yang, Ning Xu, Jianchao Yang, and Thomas Huang. Slimmable neural networks. *arXiv preprint arXiv:1812.08928*, 2018.
- [58] Sergey Zagoruyko and Nikos Komodakis. Wide residual networks. *arXiv preprint arXiv:1605.07146*, 2016.
- [59] Hong Zhang, Yupeng Tang, Anurag Khandelwal, and Ion Stoica. {SHEPHERD}: Serving {DNNs} in the wild. In *20th USENIX Symposium on Networked Systems Design and Implementation (NSDI 23)*, pages 787–808, 2023.
- [60] Jeff Zhang, Sameh Elnikety, Shuayb Zarar, Atul Gupta, and Siddharth Garg. {Model-Switching}: Dealing with fluctuating workloads in {Machine-Learning-as-a-Service} systems. In *12th USENIX Workshop on Hot Topics in Cloud Computing (HotCloud 20)*, 2020.
- [61] Minjia Zhang, Samyam Rajbandari, Wenhan Wang, Elton Zheng, Olatunji Ruwase, Jeff Rasley, Jason Li, Junhua Wang, and Yuxiong He. Accelerating large scale deep learning inference through {DeepCPU} at microsoft. In *2019 USENIX Conference on Operational Machine Learning (OpML 19)*, pages 5–7, 2019.
- [62] Barret Zoph and Quoc V Le. Neural architecture search with reinforcement learning. *arXiv preprint arXiv:1611.01578*, 2016.
- [63] Barret Zoph, Vijay Vasudevan, Jonathon Shlens, and Quoc V Le. Learning transferable architectures for scalable image recognition. In *Proceedings of the IEEE conference on computer vision and pattern recognition*, pages 8697–8710, 2018.

A Appendix

A.1 Utility of Pareto Points is Higher

Lemma A.1. *The utility of pareto-optimal subnets is higher than non-pareto-optimal subnets if they have similar inference latency for a batch of queries.*

$$\mathbb{U}(\phi_p, B, d_B) > \mathbb{U}(\phi_q, B, d_B), \quad \forall B, d_B$$

s.t. $\phi_p \in \Phi_{\text{pareto}}, \phi_q \in \{\Phi \setminus \Phi_{\text{pareto}}\}, l_{\phi_p}(B) \approx l_{\phi_q}(B)$

Proof By Contradiction. Assume a non-pareto optimal subnet (ϕ_q) such that it has higher utility than pareto optimal subnet (ϕ_p) for a batch B and $l_{\phi_p}(B) \approx l_{\phi_q}(B)$ i.e., $\mathbb{U}(\phi_p, B, d_B) < \mathbb{U}(\phi_q, B, d_B)$.

Now, due to the pareto optimal property $\text{Acc}(\phi_p) > \text{Acc}(\phi_q)$, this implies $\text{Acc}(\phi_p) \cdot |B| > \text{Acc}(\phi_q) \cdot |B|$ which implies $\mathbb{U}(\phi_p, B, d_B) \geq \mathbb{U}(\phi_q, B, d_B)$ for any delay d_B as $l_{\phi_p}(B) \approx l_{\phi_q}(B)$. This is contradiction. Hence Proved.

A.2 System Dynamics: Synthetic Traces

We also derive key observations from the dynamics to understand how SuperServe achieves high SLO attainment and better trade-offs (**R1-R2**) for synthetic traces.

Fig. 12 shows the system dynamics of SuperServe for both bursty and time-varying traces. The mean ingest rate of the bursty traces is 7000 qps and they vary in $CV_a^2 = \{2, 8\}$. Similarly, in case of the time-varying traces, the ingest rate is increased from λ_1 qps to λ_2 qps at varying accelerations $\tau = \{250 q/s^2, 5000 q/s^2\}$. The control decisions made by Slack-Fit (subnetwork (accuracy) and batch size) are shown over time.

Fig. 12a shows system dynamics for the bursty traces. The trace with $CV^2 = 8$ (blue line) has higher spikes than the trace with $CV^2 = 2$ (orange line). First, note that SuperServe operates at an accuracy range of 76 – 78% and never selects a higher accuracy subnetwork such as the subnetwork of 80.16% accuracy. This is because the subnetwork of 80.16% accuracy diverges at the mean ingest rate of 7000 qps (also seen in Fig. 8 last row). Hence, SuperServe *automatically* selects appropriate subnetworks for different mean ingest rates. Moreover, SuperServe uses lower accuracy models more frequently with increasing CV_a^2 . This is because increased jitter reduces query slack, causing SlackFit to pick lower latency buckets more often. This corroborates the trend seen in Fig. 8 where the mean serving accuracy of SuperServe monotonically decreases as CV_a^2 increases. Lastly, during the load spikes, SlackFit usually selects control parameters with high batch size and smaller subnetwork (§4.2.1). This control decision allows SuperServe to drain the queue faster, resulting in a high SLO attainment on the traces (**R1**).

Fig. 12b shows the system dynamics for the time-varying traces. $\tau = 5000 q/s^2$ (blue line) increases the ingest rate from 2500 qps to 7400 qps faster than $\tau = 250 q/s^2$. For

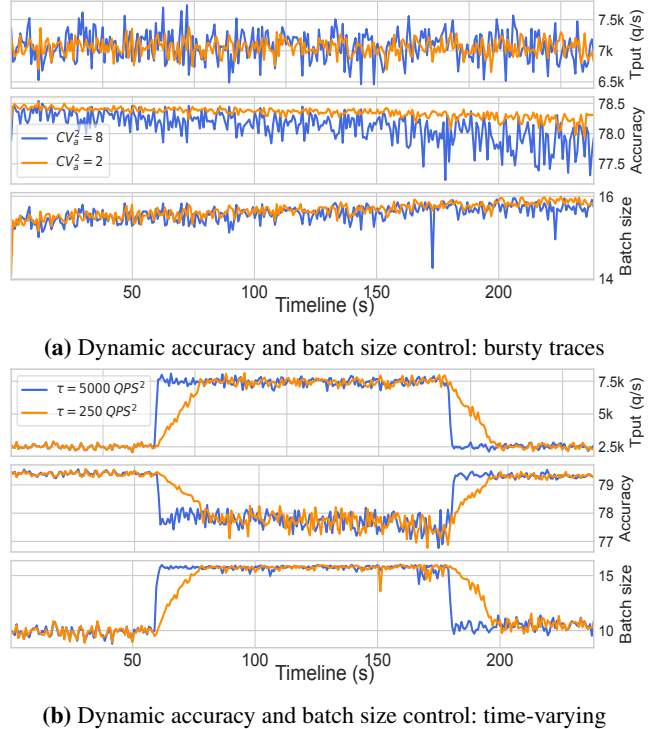


Fig. 12: System Dynamics on Synthetic Traces. Accuracy and batch size control decisions shown over time in response to ingest throughput (q/s). (a) bursty traces $\lambda = 7000 = (\lambda_b = 1500) + (\lambda_v = 5500)$ with burstiness of $CV_a^2 = 2$ (orange) and $CV_a^2 = 8$ (blue). (b) time varying traces accelerate from $\lambda_1 = 2500 q/s$ to $\lambda_2 = 7400 q/s$ with acceleration $\tau = 250 q/s^2$ (orange) and $\tau = 5000 q/s^2$ (blue). Batch size and subnetwork activation control choices over time show how SuperServe reacts to each of the four plotted traces in real time. This illustrates dynamic latency/accuracy space navigation.

both the traces, SuperServe dynamically changes the accuracy from ≈ 79.2 to ≈ 77.5 as mean ingest rate increases. SuperServe’s ability to dynamically adjust accuracy helps it achieve a higher mean serving accuracy (**R2**) compared to serving a single model statistically. Moreover, for $\tau = 5000 q/s^2$, SuperServe jumps to lower accuracy and higher batch size control parameters quickly. While, for $\tau = 250 q/s^2$, SuperServe uses intermediate models to serve the intermediate ingest rate during $\approx 60 - 80$ seconds. A higher τ value forces query’s slack to reduce drastically. Hence, SlackFit rapidly switches to selecting control parameters of smaller subnetwork and higher batch size from the low latency buckets (§4.2) to satisfy deadlines (**R1**). Therefore, increase in τ decreases mean serving accuracy (a trend observed in Fig. 9 across the rows).

A.3 Scheduling policies

The core functionality of the SuperServe’s scheduler is to maximize (a) SLO attainment and (b) prediction accuracy for any arrival trace dynamics. The scheduler offers a pluggable pol-

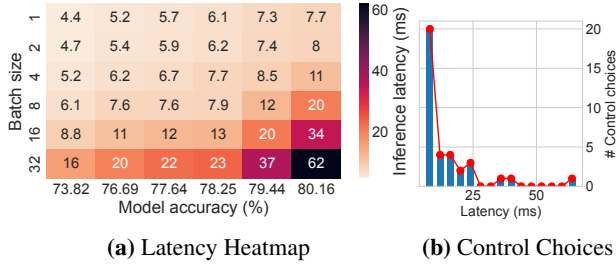


Fig. 13: SlackFit control parameter space. (a) latency heatmap for six different (uniformly sampled w.r.t. FLOPs) pareto-optimal subnets in SubNetAct as a function of accuracy (x-axis) and batch size (y-axis). The latency is *monotonic* with batch size and accuracy. (b) the number of available choices decrease as latency increases.

icy framework to support any application sensitivity to these metrics by allowing arbitrarily different trade-offs between them. SuperServe policy interface dictates that control decisions are made w.r.t. the batch size and subnetwork to activate. Both of these control parameters affect SLO attainment and serving accuracy. This is because the scheduler a) perpetually operates under a latency constraint and b) these control decisions have a cumulative effect over time (e.g., higher accuracy affects queue build-up later). Finding a globally optimal set of batch size and subnetwork control tuples over time is NP-hard. As our control decisions must be made on the critical path of queries’ end-to-end latency, quick sub-millisecond control decision making is a key performance requirement. Thus, to meet the real time requirements, we primarily consider scheduling policies that are greedy w.r.t. time. The policies decide the batch size and subnetwork based on the remaining slack of the most urgent query. The slack is calculated using a fast (sub-ms) $O(1)$ EDF queue lookup operation.

A.4 Control Parameter Space

The control parameter space of the scheduling policies is created using SuperServe’s supernet profiler (Fig. 13a) by profiling latency as a function of subnetwork accuracy and batch size. With B possible batch size choices and S different subnetworks to serve the size of the control parameter space is $B \times S$. All the scheduling policies use this space to inform their trajectory through the latency/accuracy trade-off space.

Insights. We draw some key insights from the control parameters’ space in Fig. 13a. **(I1)** the latency increases monotonically with batch size. **(I2)** the latency increases monotonically with accuracy. **(I3)** the number of control choices decreases with latency increase (Fig. 13b)⁴. These insights inform scheduling policy implementation in SuperServe. The larger batch size incurs sub-linearly higher latency, which helps increase system throughput. Thus, it is always beneficial to maximize batch size subject to the latency constraints.

⁴this occurs due to choice of power of 2 batch-size (which are granular enough to observe reasonable latency differences) and availability of fewer model choices at higher latency range.

By increasing system throughput, the systems utilization increases, serving more queries in the same amount of time, which helps the SLO attainment. At the same time, a policy may also favor more accurate subnetworks subject to query latency constraints. This increases the overall accuracy of predictions rendered by the system, improving application-visible quality of service. Thus, batch size and accuracy forms two levers of control to maximize both SLO attainment and prediction accuracy.

A.5 Policy Design Space

MaxBatch Policy. This policy first maximizes the batch size and then the accuracy. It greedily finds a maximal batch size (b) for the smallest accuracy subnetwork that fits within latency slack θ . Within the chosen batch size MaxBatch finds the maximum accuracy subnetwork (s) such that the profiled latency $L(b, s) < \theta$. It returns the control choice (b, s) . This policy leverages insights **(I1)** and **(I2)**. It takes $O(\log(B))$ operations to find b and $O(\log(S))$ operations to find s (binary search on monotonically increasing latency w.r.t. batch size and accuracy). As a result, this lightweight policy scales well with the profile table, taking only $O(\log(B) + \log(S))$ operations to make control decisions.

MaxAcc Policy. MaxAcc first maximizes the accuracy and then the batch size. Mirroring MaxBatch, MaxAcc performs a binary search for the largest accuracy (s') with $L(1, s') < \theta$ first. Then, it finds the maximal batch size (b') keeping the subnetwork choice fixed to the chosen s' , such that $L(b', s') < \theta$ ms. Similarly to MaxBatch policy, it leverages insights **(I1)** and **(I2)** and takes $O(\log(B) + \log(S))$ operations to return the control choice (b', s') .

The proposed SlackFit Policy. This is our best performing policy. At a high level, SlackFit partitions the set of feasible latencies into evenly sized latency buckets. Each bucket consists of control tuples (b, s) with $L(b, s)$ within the range of bucket width. Then the policy chooses a bucket with latency $\leq \theta$. Finally, from the choices within the selected bucket, it picks the control choice that maximizes batch size. Intuitively, selecting control parameters closest to slack θ configures the system to operate as close to capacity as possible. In other words, choices with latency less than that either reduce the throughput capacity or the serving accuracy, eventually lowering system’s SLO attainment and accuracy. This draws on the monotonicity insights **(I1)** and **(I2)**. SlackFit’s novelty is in insight **(I3)**. We observe that SlackFit *dynamically* detects and adapts to the runtime difficulty of the trace. A well-behaved trace (e.g., low ingest rate, variation, acceleration) results in higher θ . Higher θ leads to the choice of higher latency buckets. And higher latency buckets are correlated strongly with fewer control tuple choices (Fig. 13b), maximizing the probability of choosing higher accuracy models! Conversely, mal-behaved traces (higher ingest rate, variation, acceleration) lead to lower latency bucket choices, as the

scheduler is operating under much lower θ conditions. There are more control choices in lower latency buckets, which leads to control tuples within those buckets to favor higher batch sizes. This leads to processing the queue faster!

Experiment Result. In Fig. 11c we show that SlackFit achieves the best tradeoff w.r.t. our success metrics compared to both MaxAcc – a policy that greedily maximizes accuracy and MaxBatch — a policy that greedily maximizes batches. The traces used mean $\lambda = 7000$ qps ($(\lambda_b = 1500) + (\lambda_v = 5550)$) and $CV_a^2 \in \{2, 4, 8\}$. SlackFit reaches the highest SLO attainment(0.999) for all CV_a^2 . MaxBatch starts under performing w.r.t. SLO attainment with CV_a^2 increase. The SlackFit and MaxBatch difference is most pronounced at the highest CV_a^2 , eventually causing a significant 5% drop in the SLO attainment. Both policies maximize the batch size within latency slack θ when operating under small θ . When θ increases, however, MaxBatch continues to maximize the batch size unconditionally—a greedy choice that leads to packing larger batches. This greedy decision causes more time to be spent in a worker compared to SlackFit, which adaptively shifts to higher accuracy models under larger θ conditions with compound effect on queued queries, eventually missing their SLOs. maxAcc is unable to keep up with this trace. It never switches to policy decisions that process the queue faster. This policy comparison shows a continuum between faster queue processing and serving higher accuracy, with SlackFit automatically finding the best point in this continuum.

B Serving fixed accuracy points

Experiment setup. The experiments were run for the MAF trace with the mean ingest rate of 4,000 queries per second. The MAF follows a poisson-like distribution with $CV_a^2 = 1$ and the latency *SLO* for each of these requests was set to 30ms. The scheduler at the router adaptively batches the requests, along with an appropriate model based on the scheduling policy. The query-batch and model configuration is then sent to one of the 6 workers, each of which had an NVIDIA RTX 2080Ti GPU.

Results. In the plots, the red solid line represents the latency and accuracy range of all available models. Any query with remaining slack (ms) in the latency range spanned by the models can be served. It must be noted that while the system can serve queries with remaining slack higher than the right-interval red-line latency, queries with remaining slack lower than left-interval red-line latency cannot be serviced and must be dropped. The goal across policies is to manage the queue such that the remaining slack remains within the model latency range, while maximizing accuracy.

For the 6 Clipper+ experiments, the scheduler is constrained to provision all request-batches with just a single model choice. This greatly affects the system throughput, queueing delays and the SLO attainment.

- While the lower accuracy models (73.82, 76.69 and 77.64) have low inference latencies, they are able to serve the request batches within the SLO deadlines with low queueing delays. Hence they achieve 99%+ latency *SLO* attainment. This can also be seen from Fig 14 (a-c) where the remaining slack latency is right-skewed and around 30ms, which is the per-query latency deadline.
- On the other hand, higher accuracy models (78.25, 79.44 and 80.16) have significantly higher inference latencies. This leads to higher per-request serving time, higher queueing delays and lower SLO attainment. This can be seen from Fig 14 (d-f) where the distribution begins to shift leftwards towards lower remaining slack indicating significant queueing delays and lower SLO attainment.

The above results show that fixed-accuracy scheduling is insufficient to provide the best accuracy-SLO attainment trade-off across different model choices, for any given arrival-trace.

SlackFit on the other hand performs dynamic model selection throughout the models’ latency range. This provides the scheduler several choices to maximize accuracy (higher accuracy models) during low loads and also leverage the lower accuracy models during high loads. This policy serves multiple accuracy points to help absorb queue build-up and mitigate queueing delays. Since Fig 15a shows that the density function is always below the supernetwork latency range, > 99% queries meet their deadline, while also maximizing serving accuracy.

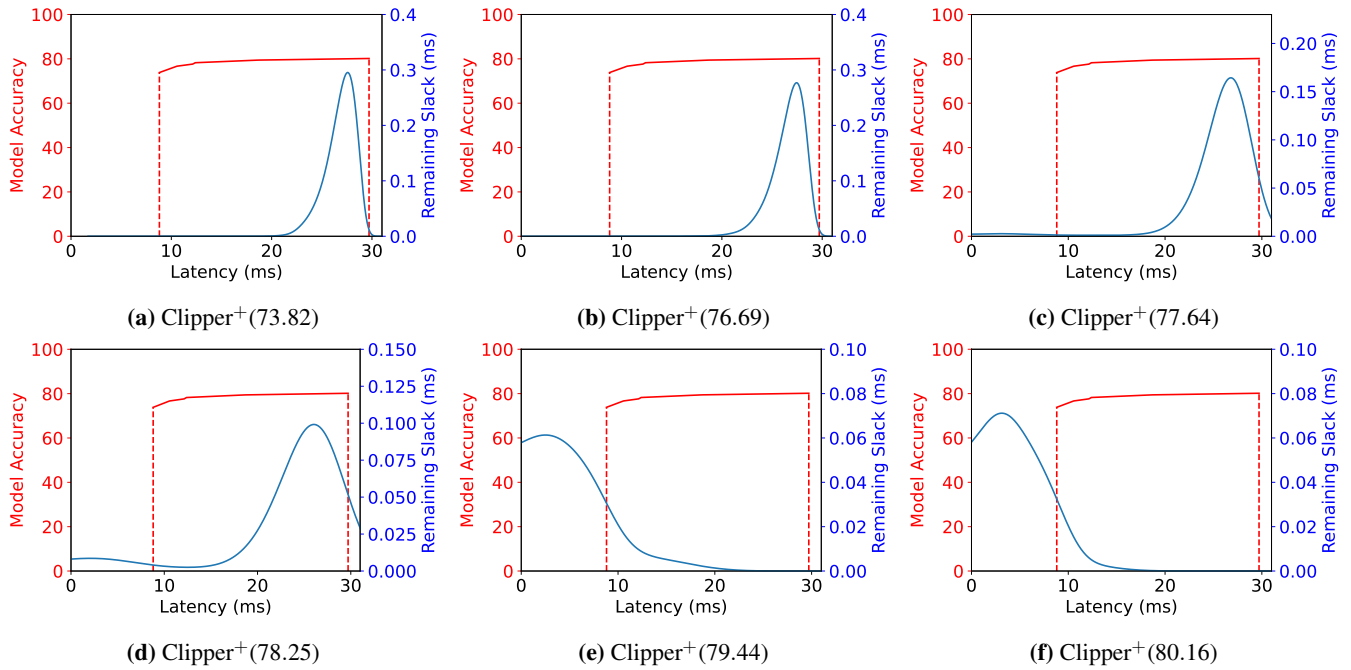


Fig. 14: Serving fixed accuracy points

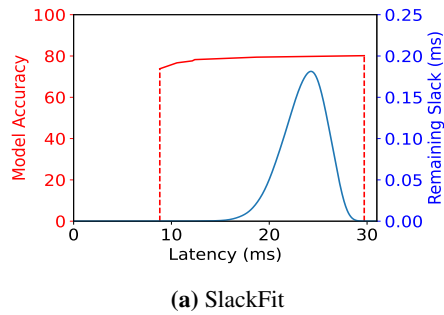


Fig. 15: Serving multiple accuracy points